nature physics

INSIGHT | REVIEW ARTICLES

PUBLISHED ONLINE: 3 MAY 2016 | DOI: 10.1038/NPHYS3736

Inertial-confinement fusion with lasers

R. Betti[1]* and O. A. Hurricane[2]

The quest for controlled fusion energy has been ongoing for over a half century. The demonstration of ignition and energy gain from thermonuclear fuels in the laboratory has been a major goal of fusion research for decades. Thermonuclear ignition is widely considered a milestone in the development of fusion energy, as well as a major scientific achievement with important applications in national security and basic sciences. The US is arguably the world leader in the inertial confinement approach to fusion and has invested in large facilities to pursue it, with the objective of establishing the science related to the safety and reliability of the stockpile of nuclear weapons. Although significant progress has been made in recent years, major challenges still remain in the quest for thermonuclear ignition via laser fusion. Here, we review the current state of the art in inertial confinement fusion research and describe the underlying physical principles.

With the advent of the current generation of high-power lasers, a high-energy-density environment can be routinely produced in the laboratory. The high energy densities produced by intense lasers are often measured in gigabars (about a billion atmospheres)—the same units as pressure. A gigabar of pressure is equivalent to 10^{14} J m^{-3} or 100 kJ mm^{-3}. The possibility of achieving such extreme pressures in the laboratory has inspired the imagination of fusion scientists since the early days of laser development. In 1972, Nuckolls[1] first published the idea of compressing a tiny target with high-power lasers to bring thermonuclear fuel to ignition conditions. In the compressed core (Fig. 1), the plasma inertia confines the plasma pressure long enough for the thermonuclear burn to produce copious amounts of fusion reactions in a process known as inertial confinement fusion (ICF)[2,3]. The largest fusion cross-section occurs for the deuterium–tritium reaction [D + T → n(14.1 MeV) + ^{4}He(3.5 MeV)], requiring temperatures of the order of several tens of million degrees or keV (1 keV ≈ 11.3 million °C) to overcome the Coulomb barrier between the fusing nuclei. Thermonuclear ignition is a thermal instability, a runaway process in the thermal energy of the thermonuclear fuel. In an ignited DT plasma, a fraction of the energy associated with the α-particles (3.5 MeV) from the fusion reactions is deposited in the plasma itself, thereby increasing its temperature and, in turn, the fusion reaction rate. The amplification of the fusion reaction rate resulting from the plasma self-heating (or alpha heating) process can lead to a fusion energy output many times greater than the input energy required to bring the plasma to ignition conditions.

If DT fuel is heated to temperatures of several keV, thermonuclear ignition occurs according to the Lawson criterion[4]. For inertial fusion, the Lawson criterion can be approximated by $P\tau > 11f(T)/\theta_\alpha$, where P is the plasma pressure, τ is the inertial confinement time of the fuel in seconds, θ_α is the fraction of α-particle energy deposited in the fuel, and $f(T)$ is a dimensionless function of the temperature T (ref. 5). For temperature profiles typical of laser-fusion capsules, the function $f(T)$ has a minimum ($f_{\min} \approx 1$) for $T \approx 15$ keV and rises steeply for $T < 10$ keV. The central temperature in the compressed core of an imploding capsule is approximately proportional to the implosion velocity ($T \sim V_{\rm imp}^{5/4}$, from hydrodynamic compression without alpha heating[6]). Because the maximum implosion velocity is constrained by the shell hydrodynamic stability[3], ignition-scale targets are designed to achieve a central temperature of about 5 keV before ignition occurs. At 5 keV, the function f (5 keV) ≈ 2.6 and laser-fusion targets require $P\tau \gtrsim 36$ atm s for ignition at 5 keV with $\theta_\alpha \approx 0.8$, about three times the value required for magnetically confined tokamak plasmas operating at temperatures above 10 keV. The ignition process starts from the central low-density hot plasma (called the hotspot), whereas most of the fuel is contained within a dense compressed shell surrounding the hotspot (Fig. 1). The dense shell provides the principal source of mass for the hotspot and the inertial confinement of the high central pressure. The confinement properties depend on the areal density of the compressed core, $\rho R \equiv \int_0^R \rho {\rm d}r$, which is routinely measured in implosion experiments[7–9]. The areal density is controlled by varying the entropy of the fuel, which is determined by the fuel adiabat, defined as the ratio of the pressure to the Fermi-degenerate pressure (adiabat = $P/P_{\rm Fermi}$ (ref. 3)). The lower the adiabat, the higher is the areal density of the compressed fuel. For a uniform spherical compression, the Lawson ignition criterion can also be expressed in terms of the total areal density and temperature as $\rho R(T/4.7)^{2.2} > 1$ (ref. 5), where ρR is in g cm^{-2} and T is in keV (without alpha heating). This form of the ignition condition indicates that ignition requires large enough areal densities (low adiabat) and hot enough cores (high velocity). However, fast targets imploded on a low adiabat are susceptible to hydrodynamic instabilities that drive the rapid growth of nonuniformities on the capsule surface, leading to severe degradation of the final compression and quenching of the ignition process[10]. The growth of these instabilities can be controlled by reducing the velocity and/or increasing the adiabat at the price of reducing the final compression. Striking the right balance between compression and stability to achieve the highest Lawson parameter $P\tau$ is of crucial importance to the success of inertial fusion.

So far, laser-fusion implosions at the National Ignition Facility (NIF)[11,12] at the Lawrence Livermore National Laboratory (LLNL) have achieved more than half of the value of $P\tau$ required for ignition (over 20 atm s; as shown in Fig. 2 where the implosion stagnation pressure is determined from the measured neutron yield, image data reconstruction of the hotspot volume, neutron-time-of-flight inferred $T_{\rm ion}$, and diagnosed burn width τ using a technique similar to refs 13–15). Although ignition remains an elusive goal, NIF implosions have demonstrated, for the first time, a fusion yield exceeding the total energy (thermal and kinetic) of the DT

[1]Laboratory for Laser Energetics, University of Rochester, Rochester, New York 14623, USA. [2]Lawrence Livermore National Laboratory, Livermore, California 94550, USA. *e-mail: betti@lle.rochester.edu

NATURE PHYSICS DOI: 10.1038/NPHYS3736

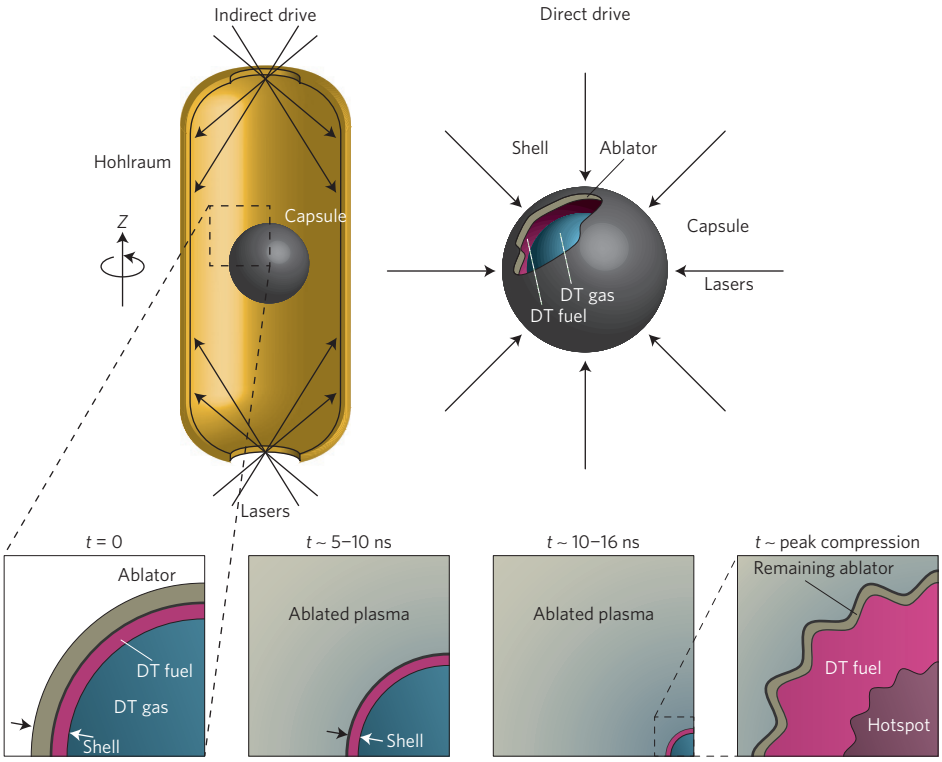

Figure 1 | Schematics of indirect- and direct-drive ICF. Typical targets used in laser-driven ICF are indirectly driven (upper left) or directly driven (upper right). In either case, a spherical capsule is prepared at $t = 0$ with a layer of DT fuel on its inside surface. As the capsule surface absorbs energy and ablates, pressure accelerates the shell of remaining ablator and DT fuel inwards—an implosion. By the time the shell is at approximately one-fifth of its initial radius it is travelling at a speed of many hundreds of kilometres per second. By the time the implosion reaches minimum radius, a hotspot of DT has formed, surrounded by colder and denser DT fuel.

fuel[13]. In these implosions, self-heating from fusion α-particles has been estimated to enhance the plasma thermal energy, leading to a doubling of the fusion yield[16–18]. Ignition-scale implosions on the NIF use the indirect-drive approach[3], where the laser irradiates the inner walls of a high-Z metal enclosure (hohlraum) to produce X-rays. The spherical capsule, approximately 1 mm in radius, is positioned inside the hohlraum and consists of an outer plastic (or other low-Z material) shell (the ablator) enclosing an inner layer of cryogenic solid DT (Fig. 1). The X-rays incident on the capsule outer surface cause mass ablation off that surface, leading to an inward momentum input (rocket effect) driving the implosion. In the best-performing indirect-drive implosions on the NIF (the so-called 'High-Foot' targets[13,16]), the DT mass has been accelerated with 1.9 MJ of ultraviolet light to about 360–380 km s^{-1}, reaching a fuel kinetic energy of about 12 kJ and producing about 26 kJ of fusion energy. At present, low-mode (in spherical harmonics $Y_\ell^m(\theta,\phi)$, modes ℓ and $m \lesssim 4$ are 'low') asymmetries in the X-ray drive are believed to be the leading, but not the only, cause of performance degradation in indirect drive. Improvements in implosion symmetry, X-ray conversion and capsule hydrodynamic stability are thought to be within reach and sufficient for a significant step forward in implosion performance. The experimental campaign to achieve ignition on the NIF is a collaborative effort between the institutional partners Lawrence Livermore National Laboratory, University of Rochester, Los Alamos National Laboratory and Sandia National Laboratories, as well as other collaborators such as General Atomics, which makes the fusion targets, and the Massachusetts Institute of Technology, which develops nuclear diagnostics. A laser facility with capabilities similar to the NIF, the Laser MegaJoule[19], is being built at present near Bordeaux (France) by the French Atomic Energy Agency (Commissariat à l'Energie Atomique, CEA).

In addition to the indirect-drive effort at the NIF, the US laser-fusion programme also relies on the direct-drive approach, mostly developed on the OMEGA laser[20] at the Laboratory for Laser Energetics (LLE) of the University of Rochester and the Nike laser[21] at the Naval Research Laboratory (NRL). Outside the US, important research work in direct drive is conducted at Osaka University in Japan, the Research Center for Laser Fusion in China, the University of Bordeaux in France, the University of Rome in Italy, and smaller efforts throughout Europe (including Russia) and Asia. In direct drive, the spherical shell is directly irradiated by the laser incident on the capsule outer surface. With respect to indirect drive, direct drive exhibits higher conversion efficiency from laser energy to shell kinetic energy, thereby allowing an implosion of greater DT fuel mass. A disadvantage of direct drive is the reduced uniformity of the illumination. Whereas the bath of X-rays in the hohlraum is free of small-scale nonuniformities, laser beams exhibit speckle patterns with large variations in laser intensity. In direct drive, this leads to imprinting of small-scale laser-intensity patterns on the target surface[22–24]. During the implosion, hydrodynamic instabilities drive the rapid growth of such nonuniformities, leading to reduced final compression and, in some cases, breakup of the shell while in flight. Similarly to indirect drive, the implosion performance of directly driven targets can also be degraded by low-mode asymmetries. In direct drive, low-mode asymmetries are seeded mostly by the finite number of overlapping incident laser beams and the power imbalance between beams (so, in the direct-drive context, 'low modes' are ℓ and $m \lesssim 10$). Another source of degradation comes from the laser–plasma instabilities[25] occurring when the laser light interacts with the ablated plasma. These instabilities can limit the absorption of the laser energy and accelerate plasma electrons that can reach the DT fuel. Energetic (hot) electrons can heat up the DT fuel layer while in flight (preheating[26]), thereby

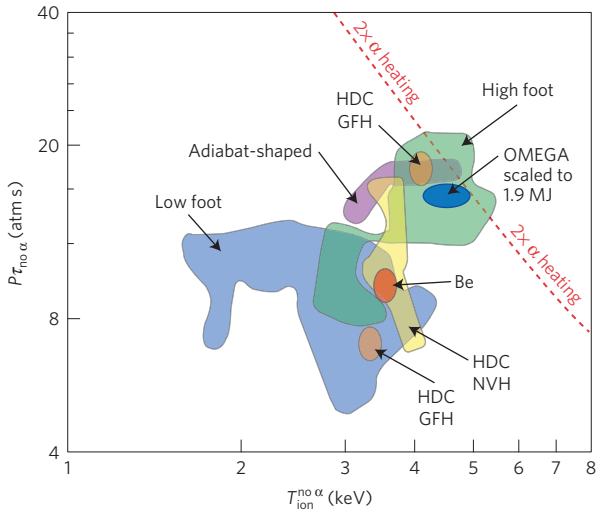

Figure 2 | Performance of indirect- and direct-drive ICF in terms of the Lawson parameter $P\tau$ and ion temperature T_{ion}. The different colour-coded bubbles envelope the data from various indirect-drive campaigns on NIF up to July 2015 with energies up to 1.9 MJ. The HDC gas-filled hohlraum (GFH) campaign is distinguished from the HDC near-vacuum hohlraum (NVH) campaign. Direct-drive implosions are carried out on OMEGA using 26 kJ of laser energy, and their performance is extrapolated to 1.9 MJ using the hydrodynamic scaling[28]. The figure shows OMEGA implosions in April–November 2015[27]. The dashed red line marks the requirements for doubling of the fusion yield from alpha heating. Both $P\tau$ and T_{ion} are values estimated from pure hydrodynamic compression without accounting for alpha deposition (no α (refs 5,17,39)).

reducing the final compression and preventing the onset of the ignition process.

Because of the energy limitations of the OMEGA laser (30 kJ of ultraviolet light), direct-drive targets on OMEGA are much smaller than indirect-drive targets on the NIF. The DT mass in OMEGA targets is about ten times less than in present NIF targets. To assess the performance of direct-drive OMEGA implosions, their value of the Lawson parameter $P\tau$ is theoretically extrapolated to the larger targets that could be imploded in the future with the same energy of 1.9 MJ used at present for indirect drive on the NIF. It is found that, when scaled to 1.9 MJ, existing direct-drive implosions[27] would not achieve ignition. It is estimated that direct-drive targets scaled to 1.9 MJ would exhibit levels of alpha heating (Fig. 2) similar to those of current indirect-drive targets measured by an amplification of the fusion yield of about 2× (ref. 28). Techniques to mitigate the effect of laser–plasma instabilities, to improve the laser-energy absorption and to reduce the seeds of hydrodynamic instabilities are being investigated with the goal of producing an implosion on the OMEGA laser that would scale to ignition when extrapolated to the 1.9 MJ of the NIF.

Alternatives to the conventional direct- and indirect-drive schemes described above are also being investigated in the US, Europe, Japan and China. These advanced concepts separate the fuel compression from ignition. The two-step process uses a conventional scheme (direct or indirect drive) to assemble the DT fuel into a compressed dense core using a slow implosion. Slow implosions are less susceptible to the detrimental effects of hydrodynamic instabilities, and require lower laser intensities, making them less prone to exciting laser–plasma instabilities. Because of the relatively low central temperatures and pressures achieved in low-velocity implosions, the compressed core requires an additional external energy input to trigger the ignition process. This can be provided by an energetic particle beam (electrons or ions) produced by the interaction of a short (picosecond) and intense ($\sim 10^{19}$–10^{20} W cm^{-2}) petawatt laser pulse (fast ignition[29]) or by a strong spherically convergent shock wave launched by a spike in the laser intensity (up to $\sim 10^{16}$ W cm^{-2}) at the end of the implosion (shock ignition[30]). Both fast and shock ignition have made significant progress in recent years. Fast-ignition-integrated experiments have shown a considerable fusion yield enhancement from the heating from the petawatt laser pulse[31,32]. Shock ignition experiments[33] have demonstrated shock-driving pressures well above 300 Mbar, and a significant increase in shock strength due to hot electrons—from laser–plasma instabilities—slowing down in the target. However, uncertainties in the laser–plasma interaction physics at high intensities have prevented a conclusive evaluation of the viability of these schemes.

Another advanced ICF scheme uses targets embedded in magnetic fields to reduce the heat losses within the DT fuel. The magnetized targets can be laser-driven (magnetized ICF[34]) or imploded with a pulsed-power device (z-pinch fusion). Pulsed-power devices have been widely used for z-pinch implosions since the early days of fusion research. Recently, a new approach known as magnetized liner inertial fusion[35] (MagLIF) has combined z-pinch implosions and laser heating of cylindrical targets embedded in an axial magnetic field. Recent MagLIF results from Sandia National Laboratories have demonstrated significant fusion yields and magnetic confinement of the fusion products[36].

In summary, significant progress in implosion performance has been made in laser fusion over the past few years. Fusion yields exceeding the total energy input to the DT fuel, as well as significant contributions from alpha heating, have been demonstrated on the NIF. Estimates for the effect of alpha-heating power relative to the input work rate to the central hotspot (during the compression phase up to stagnation) indicate that alpha heating is responsible for over one-third of the total input energy to the fusing hotspot plasma[17].

Laser indirect drive

The physics basis for indirect-drive ignition on the NIF has been documented previously[3,37,38], as was the subsequent outcome of the National Ignition Campaign (NIC)[39]—the three-year effort to achieve ignition from 2009 to 2012. The NIC implosion focused on a design that emphasized maximizing fuel ρR for the purpose of minimizing the energy required for ignition and achieving high gain. Maximizing fuel ρR also increases the margin against failing to ignite, but only when the implosion behaves in an ideal nearly one-dimensional way (uniform spherical implosion).

The DT implosion targets in the NIC largely focused on a 195-μm-thick CH (carbon–hydrogen, plastic) ablator with a nominal outer radius of 1,143 μm, a 70-μm thickness of DT fuel inside a 0.96 mg cm^{-3} helium-gas-filled (to slow the ingress of hohlraum plasma) gold hohlraum, 5.75 mm in diameter and a centimetre in length. Arriving at this particular design choice was a complex process that took place over a decade, but the basic rationale can be simply understood. The hohlraum material needs to be high-Z and high density to have high opacity to X-ray radiation and minimize the diffusion of radiant energy into the wall of the hohlraum—this maximizes the energy coupling to the capsule. Au is both high-Z and high density while being readily available and easily manufacturable. The surface area of the hohlraum is determined by the required radiation temperature, T_{r}, and the laser power (P_{laser}) delivery capability of the facility, largely through the relationship, $P_{\text{laser}} \sim \sigma T_{\text{r}}^4 A_{\text{hohlraum}}$, where σ is the Stefan–Boltzmann constant and A_{hohlraum} is the inside surface area of the hohlraum. The diameter of the laser entrance holes (see Fig. 3a) must be large enough to accept the cross-section of the laser beams entering the hohlraum, yet not so large as to be a significant source of radiant energy loss, which would reduce T_{r}. The length, diameter and geometry of the hohlraum, along with the specific beam pointing, are chosen to best control the low-mode symmetry of the implosion. The ratio

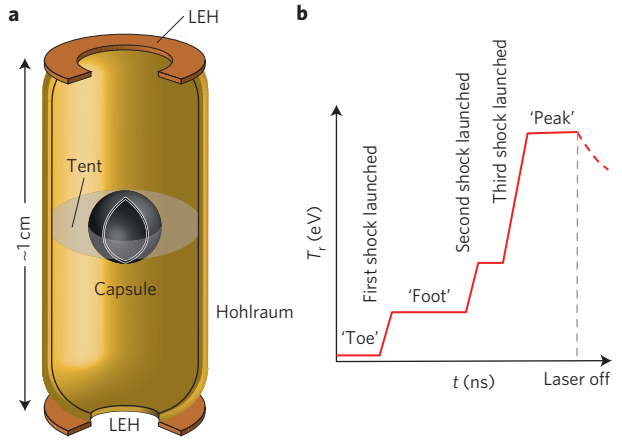

Figure 3 | Indirect-drive target and laser pulse. a, A cut-away image of a typical indirect-drive target for NIF is shown with some key components identified. The cylindrical hohlraum encloses the ICF capsule supported by a thin (15–100 nm) membrane (the tent). Laser beams enter the hohlraum through the laser entrance holes (LEHs) and are incident on the inside of the wall of the hohlraum. Generally, the volume of the hohlraum that is not occupied by the capsule is filled with helium gas, the density of which is dependent on the design, but generally ranges from 0.03 to 1.6 mg cm^{-3}. The helium gas is contained in the hohlraum by plastic windows at the LEH (not shown). **b**, A schematic three-step/three-shock radiation drive noting the nomenclature for the different phases of the drive. The toe of the drive is used to vaporize the plastic windows covering the LEH before significant laser energy is delivered to the target.

of hohlraum inner diameter to capsule outer diameter (often called the 'case-to-capsule' ratio) is another important consideration for uniform X-ray illumination of the capsule and implosion symmetry.

In combination, T_r and ablator material properties, $\bar{A}$ and $\bar{Z}$, which are the average atomic mass and the average atomic charge number, respectively, determine the ablation pressure, $P_{abl} \sim \sqrt{(\bar{A}/(\bar{Z}+1))}T_r^{3.5}$ (arrived at by equating the mechanical power per unit area in the rarefied ablation region, $P_{abl}c_{sound}$, to the incoming radiant power per unit area, σT_r^4, with c_{sound} being the sound speed), as the front of X-ray radiation ionizes the material and accelerates the implosion inwards on itself. Plastic is a reasonable choice of ablator, being a compromise between P_{abl}, a low enough opacity to allow X-ray radiation to penetrate its surface, and manufacturability. High-density carbon (HDC), beryllium (Be) and boron-carbide (B_4C) are generally superior ablator materials to plastic in terms of ablation pressure and rocket efficiency, but their crystalline structure poses manufacturing and potential hydrodynamic instability challenges.

The laser pulse used in indirect drive is generally designed to create a T_r versus time (the X-ray radiation 'drive' history) that increases in steps (see Fig. 3b), with each step in T_r generating a large step in P_{abl} that launches a radially convergent shock into the capsule. The duration and level of the steps in T_r determine the adiabat, implosion speed, and stability of the implosion through the time history of P_{abl}. For the NIF indirect-drive implosions, characteristic peak levels of T_r and P_{abl} are $\sim$300 eV and $\sim$100 Mbar, respectively. The first step-up in T_r is generally referred to as the 'foot' of the radiation drive. For the NIC implosion, also known as the 'low foot', which had four steps in T_r, and therefore was a four-shock implosion, the foot level was $T_r \sim 60$ eV for a duration of about 10 ns out of a total pulse duration of about 22 ns.

The results of the NIC suffered from greater than anticipated ablation-front instability, primarily from unstable growth to a large amplitude of baroclinic vorticity ($\nabla\rho \times \nabla P/\rho^2$) (ref. 40) seeded by the 'tent' membrane[41] around the two circles where the tent loses contact with the capsule surface (Fig. 3a), perhaps additionally aggravated by underestimating the initial seeds for growth[42] on the capsule surface. Additional degradation in implosion performance originated from mixing of ablator material into the implosion hotspot for shots with implosion speed above $\sim$320 km s^{-1} (refs 43–46; in ref. 43 the Cu and Ge dopants placed at different radial locations in the plastic ablator show the ablation-front hydrodynamic instability is primarily responsible for hot-spot mix), hohlraum-driven time-dependent implosion symmetry control problems[47,48], and a persistent drive deficit problem[49] (where X-ray energy in the hohlraum seems to be missing from the system) that is at least partially due to not correctly predicting hohlraum radiation hydrodynamics[50]. The degree to which each of the above effects contributed to the observed performance of the NIC implosion is best understood at present from fully three-dimensional high-fidelity simulations[40]. Herein, we concentrate on the status and prospects based on the past few years of progress and scientific exploration on the NIF, which leverage the remarkable diagnostic suite developed under the aegis of the NIC.

Since 2012, progress has been made towards ignition conditions (see Fig. 2) by using pulse shapes that are resistant to hydrodynamic instabilities, such as the ablative Rayleigh–Taylor (A-RT) instability, over a range of ablator materials, pulse shapes and hohlraum gas fills. Because the 'foot' of the X-ray drive determines the strength of the first shock, it is mostly responsible for setting the adiabat of an indirectly driven implosion. The shell adiabat affects the density gradient scale length, L_ρ, and the in-flight density of the ablator, which in turn gives the foot level the ability to alter the A-RT instability growth rate (for example[2], assuming radial symmetry),

$$\gamma_{\text{A-RT}} = \alpha_2\sqrt{\frac{\ell g/R}{1+\ell L_\rho/R}} - \beta_2\frac{\ell}{R}v_{abl} \qquad (1)$$

where $g = P_{abl}/(\rho\Delta R)$ is the shell acceleration (with ΔR the shell thickness and ρ the shell density), R is the shell radius, v_{abl} is the ablation velocity, which increases with T_r, and α_2 and β_2 are coefficients of order unity. So, by raising the level of the foot, such as in the so-called 'High-foot' implosions, the instability growth rate is reduced by the increase in both L_ρ and v_{abl}. High modes (ℓ in the range from many tens to hundreds) are very effectively controlled with a high-foot-like drive. The trade-off in raising the foot is that the shell will converge less owing to the higher adiabat, thereby reducing the theoretical final compression. Lower convergence ratios $CR = R_{initial}/R_{final}$ lead to lower theoretical core pressures and areal densities when the shell stagnates. However, lower convergence ratios reduce not only the growth of high-mode Rayleigh–Taylor modes, but also the growth of low-mode asymmetries that are amplified by convergence effects.

In a strategy of performing implosions that are less impacted by high-mode Rayleigh–Taylor instability growth and less sensitive to low-mode drive asymmetries (using high-foot-like drives), combined with making small systematic steps in a complex parameter space of initial conditions, notable accomplishments have been:

- Achieving more than a doubling of the fusion yield due to α-particle self-heating and fusion neutron yields of 26 kJ (refs 16–18,51).
- Demonstrated mitigation of the ablative Rayleigh–Taylor instability via laser pulse-shape modifications[52–56] in a way that was consistent with theoretical/simulation expectations[40,57,58].
- Demonstration of DT implosions that range in levels of fuel compression from $\rho R = 0.6$ g cm^{-2} to $\rho R = 1.1$ g cm^{-2} (refs 59–66) with fuel velocities in excess of 380 km s^{-1} (refs 16,51,67), with no indications of mixing of ablator material into the hotspot.

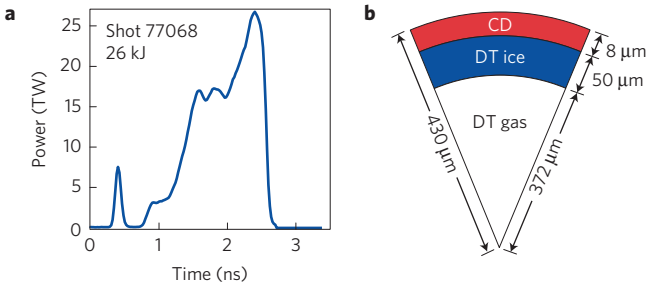

Figure 4 | OMEGA direct-drive target and laser pulse. a, Time evolution of a 26-kJ laser pulse. **b**, The target used in cryogenic implosion experiments on OMEGA, showing the CD plastic ablator layer, the cryogenic fuel layer (ice) and the DT vapour (gas).

- Demonstrating stagnation pressures in excess of 200 Gbar (refs 16,51) at temperatures of about 5 keV.

However, in the process of obtaining the above results, a significant proportion of the data suggests that the higher-convergence and higher-velocity indirectly driven implosions of the NIF are not behaving like the ideal 'text-book'[2,3] implosion in spite of mitigating the growth of hydrodynamic instabilities. This deviation from ideal behaviour was not entirely unexpected, because numerous issues were suspected in degrading the performance of NIC implosions, and mitigating the A-RT instability addressed only one (dominant) issue. These newer A-RT-mitigated and less-convergent implosions on NIF serve as integrated diagnostics of the remaining difficulties.

As was documented in a series of experiments that incrementally increased laser drive on high-foot implosions[59,60], symmetry of the implosions' central hotspot degraded as laser power was increased in hohlraums with 1.6 mg cm^{-3} of helium gas fill, resulting in oblate, and sometimes even toroidal hotspots. Typically, high laser power leads to high implosion speeds. However, increased laser power also leads to greater potential laser–plasma instability (LPI) and intense ablation of the hohlraum wall where the laser spots land. Whether LPI was diverting laser energy away from the waist (middle circumference) of the hohlraum or whether high-Z plasma plumes emanating from the laser spots on the wall were interfering with the path of the laser beams is still unclear. However, at the time it was reasoned that reduced laser power, although significantly increasing the duration of the laser pulse at peak power, would allow the capsule to achieve high velocity while also reducing the chance of unpredictable hohlraum behaviours.

Indeed, increasing the delivered laser energy by lengthening the time duration of the laser pulse at peak power as a means to increase implosion speed, instead of laser power, appeared to be preferable in terms of hotspot symmetry control and net fusion performance, in contradiction to the conventionally expected behaviour. A key element of managing implosion symmetry in the high-gas-fill hohlraum was a reliance on manipulating cross-beam energy transfer (CBET). CBET is the process of energy transfer mediated by low-gain stimulated Brillouin scattering (SBS) between crossing laser beams. This laser–plasma instability was used to force more energy onto the middle circumference of the hohlraum[68–71]; however, there are limits to this technique, as there are limits to the maximum amount of energy the laser itself can supply. Moreover, even after years of using CBET to successfully manage gross aspects of implosion symmetry in practice, considerable uncertainty exists surrounding the detailed time dependence of the energy transfer, and the modelling capability for CBET is in its development stages.

Further improvements in hotspot symmetry control and net fusion performance were obtained by transitioning from a gold (Au) to a depleted uranium (DU) hohlraum[16]. For a fixed amount of laser drive, DU effectively increases the peak T_r, and therefore the ablation pressure. DU atomic physics differences (lower opacity than Au at ∼100 eV temperatures and higher opacity than Au at ∼300 eV temperatures) also appear to increase the emissivity at the hohlraum waist, thereby driving the waist of the implosion slightly harder than in Au, and reducing the tendency towards oblate implosions[71]. To a certain extent, reducing the ablator thickness was also effective at improved symmetry control and net fusion performance[67]. Thinner ablators, although risking more instability because of increased in-flight-aspect-ratio (IFAR = $R/\Delta R$), yield a higher implosion speed for a given peak T_r and also inject less ablator plasma into the hohlraum, thereby facilitating the propagation of the laser beams. Although fusion yields and stagnation pressures increased as the implosion velocity was increased, and reproducibility of nuclear performance was demonstrated[67], eventually a performance maximum and cliff were identified[51]. The observed performance cliff showed no evidence of hotspot mix, but low measured optical depth along at least one diagnostic line of sight, suggesting localized regions of low areal density ('thin spots') in the shell of the implosion that resulted in a loss of confinement as the high central pressure hotspot burst through the thin regions of the shell[18].

The results from integrated two-dimensional post-shot simulations of the high-foot target series[72] and three-dimensional simulations[73] are largely consistent with experimental data, and imply that implosion asymmetry is a key mechanism responsible for the measured fusion performance of the high-foot targets, but not the only mechanism (the tent and three-dimensional features seem to be of increasing importance for the high-velocity high-foot experiments). Furthermore, although mitigating the A-RT reduces the damage to the implosion coming from the tent mounting membrane, data indicate the hotspot[74] and shell[75] of the high-foot implosions are still impacted. Hot electrons[76] are another potential source of asymmetry. Regardless of their origin, asymmetries degrade the conversion of kinetic energy of the imploding fuel shell into internal energy at stagnation[72,77] and, if severe enough, can lead to a loss of confinement through 'thin spots' that develop in the fuel and remaining ablator. Data and post-shot simulations indicate that, at present, many indirectly driven NIF implosions have poor shell symmetry[78–80] even when the hotspot appears fairly round, regardless of ablator or pulse shape.

Remarkably, experiments using alternate and more efficient ablator materials such as Be (motivated by its low opacity, which makes it a superior X-ray absorber, and high ablation pressure)[81,82] (J. Kline, *et al.* manuscript in preparation) or HDC (motivated by its high ablation pressure and relatively high density)[63] had the same essential fusion performance as CH ablators when driven by the same gas-filled hohlraum and high-foot pulse shape, even having the same observed hotspot shape in the case of HDC[66]. These results imply that the gas-filled hohlraum is dominating the performance of these implosions.

Attempts at retaining the good hydrodynamic stability properties of the high-foot targets, while returning to the higher levels of compression of the NIC implosion via adiabat shaping[58,83,84], were successful in increasing the fuel ρR by ∼20%, from where the high-foot fuel ρR saturated in a high-gas-fill hohlraum[61,62,85], and in greatly reducing the signatures of hot electrons effusing from the hohlraum (at 350 TW and 1.6 MJ of laser power and energy). However, the fusion yield performance and inferred stagnation pressure were essentially not improved as compared to high-foot implosions with equivalent target geometry and laser drive—again consistent with the picture of significant ρR variations in the shell being unable to confine the high-pressure hotspot. These results suggest that the dense fuel-shell and central hotspot properties are not as coupled as one would expect for a uniform one-dimensional implosion. At higher laser drive (388 TW and 1.74 MJ) and with a thinner (175 μm) ablator, the total neutron yield and fuel ρR

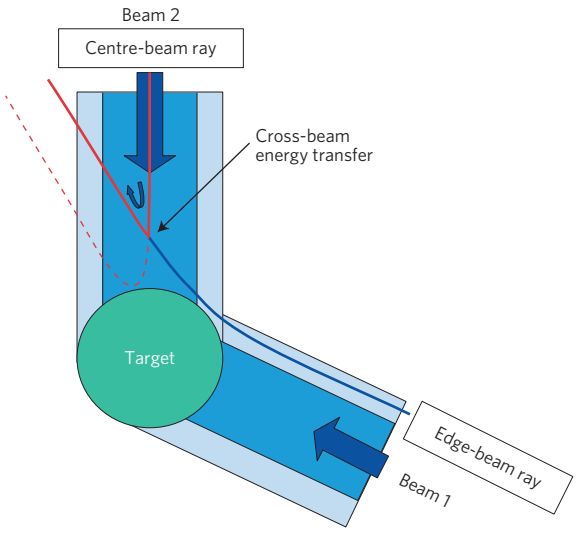

Figure 5 | Schematics of the CBET process. Laser rays from the edge of a beam graze the target and cross incoming rays from the central portion of another beam. Laser energy is transferred from the incoming to the outgoing rays, reducing the laser-energy deposition on target. Figure reproduced from ref. 107, American Institute of Physics.

were comparable, to within error bars, for adiabat-shaped and equivalently driven high-foot shots[86], perhaps as a result of late-time hot-electron preheat.

Larger case-to-capsule-ratio (the ratio of inner hohlraum wall and outer capsule radii) near-vacuum hohlraums, which are well suited to the very short laser-pulse durations of the HDC ablator, have shown ∼98% levels of laser-to-hohlraum energy coupling (resolving the aforementioned 'drive deficit' problem), the ability to control symmetry directly through laser cone fraction without needing CBET, and a reduction of hot electrons by a factor of 100–1,000× (over an energy range of 50–300 keV) than in high-gas-fill hohlraums[64,65]. The addition of a small amount of helium gas (0.3–0.6 mg cm^{-3}), for a low-gas-fill hohlraum configuration, makes it possible to use less efficient ablators such as CH, yet retain much of the benefit of the near-vacuum hohlraum[87]—a direction which indirect-drive work on NIF is at present developing to address the obstacle of implosion shape control. Work on hohlraums with alternative geometries (for example, the 'rugby'), which have also demonstrated low hot-electron levels, is also continuing, in close collaboration with CEA in France[88].

Work to clearly assess and mitigate the negative impact of engineering features in contact with the capsule is also just developing. Once the major challenges of implosion time-dependent shape control and capsule mounting features are addressed, it is anticipated that other challenges will emerge from the data. Experiments that back away from highly stressing (for example, high convergence ratio) implosions will be pursued to assess where numerical simulations depart from observation and determine what improvements are needed in our predictive capability. In parallel, efforts focusing on delivering more energy to the imploding DT fuel (designs that achieve >430 km s^{-1} implosion speeds emphasizing high hotspot ρR), which lessens the need for high finesse, will also be developed.

Laser direct drive

Direct laser illumination of the capsule surface (direct-drive ICF) has the advantage of maximizing the energy coupled to the imploding DT fuel. Direct drive couples to the DT fuel about five to six times more energy than indirect drive. For instance, a capsule imploded by 2 MJ of direct ultraviolet laser irradiation is expected to acquire about 80–100 kJ of fuel kinetic energy compared to ∼12–16 kJ of existing indirect-drive NIF targets. Because of the better laser-energy coupling, direct drive can assemble a greater fuel mass than indirect drive. Some disadvantages of direct drive with respect to indirect drive include: greater drive nonuniformity, especially at small scales (much smaller than the capsule size), and a thinner ablator layer. Because of the low mass ablation rate for direct irradiation, direct-drive capsules use a thinner ablator layer than indirect drive, thereby providing relatively less protection of the inner DT fuel layer from hot-electron and/or radiation preheating.

Laser-smoothing techniques have been adopted to improve the laser-beam uniformity, and the laser intensity is maintained slightly below a critical value (∼10^{15} W cm^{-2}) to control laser–plasma instabilities. In the US, direct-drive experiments have been conducted on the OMEGA[20] and Nike[21] lasers. Very recently, direct-drive experiments have been fielded on the NIF to study laser-to-target energy coupling, laser-drive asymmetries[89,90] and laser–plasma instabilities in long-scale-length plasmas[91]. Cryogenic implosions have been carried out on the OMEGA laser since 2000[92]. After an initial phase where the fuel was pure deuterium, OMEGA implosions have used a deuterium–tritium mixture[93] since 2006. The implosion performance is assessed through the Lawson parameter (described earlier), the central pressure, the central temperature, the neutron yield and the areal density.

The main accomplishments so far of the direct-drive effort on OMEGA cryogenic implosion experiments are:

- Demonstrating hotspot pressures in excess of 50 Gbar at temperatures of about 3.6 keV and neutron yields of about 5 × 10^{13} with approximately 26 kJ of laser energy[27].
- Demonstrating close to one-dimensional areal densities of about 0.2 g cm^{-2} at adiabats of ∼4 and implosion velocities of about 360 km s^{-1} (ref. 27).
- Demonstrating implosion performance that scales hydrodynamically to alpha-heating levels of about 2× in yield amplification at 1.9 MJ of laser energy[28].

Typical OMEGA implosions use about 26 kJ of ultraviolet laser energy on target, with intensities of about 8 × 10^{14} W cm^{-2} and pulse lengths of a few nanoseconds (Fig. 4a). The highest performance targets are spherical shells (outer diameter 860 μm) with an 8-μm-thick CD plastic ablator and a 50-μm-thick inner layer of DT ice (Fig. 4b). Single or multiple decaying shocks are launched by pickets[94–96] in the laser power at the beginning of the pulse. The main pulse, with most of the 26 kJ of laser energy, follows the pickets. The decaying shocks combined with the shock from the rising part of the main pulse are used to produce a monotonically decreasing entropy (or adiabat) profile within the shell that is maximum on the outer surface and minimum on the inner surface (adiabat shaping[94,95]). Keeping the inner portion of the DT fuel on a low adiabat minimizes the energy required to compress the fuel to high densities. High adiabat values on the outer surface lead to lower ablation-front densities, thereby augmenting the penetration velocity of the ablation front into the shell (ablation velocity). Higher ablation velocities slow the growth of hydrodynamic instabilities that develop on the ablation front when the shell is accelerated inwards[97]. Typical laser pulses for direct drive are designed to shape the adiabat with an outer value about 2× above the inner value. The best performance so far was obtained for inner values of the calculated adiabat of about 3 to 4. A 26 kJ laser pulse ablates all the plastic ablator and a fraction of the DT fuel to accelerate the unablated DT (about 18 μg) to a peak implosion velocity of about 360 km s^{-1} with a kinetic energy of ∼1.2 kJ. The imploding shell is slowed down by the build up of pressure in the centre as the shell converges. At stagnation, the shell is highly compressed to densities of a few hundreds of grams per cubic centimetre, surrounding the

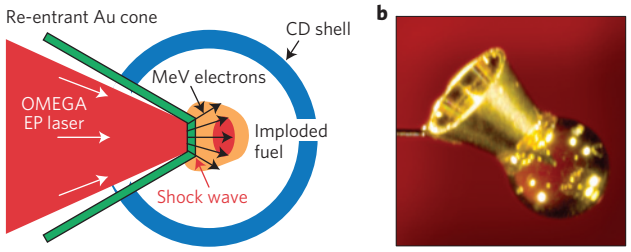

Figure 6 | OMEGA fast-ignition targets. a, Schematics of the cone-in-shell electron-fast-ignition experiments on the OMEGA laser facility. **b**, The cone-in-shell target used in integrated FI experiments on OMEGA. Figure reproduced from ref. 31, American Institute of Physics.

lower-density hotspot plasma. In recent OMEGA experiments[27], the hotspot achieves a 3–4 keV temperature and over 50 Gbar of pressure—high enough to trigger tens of trillions of fusion reactions (up to about 5×10^{13}). The fusion burst lasts for about 60–70 ps before the hotspot cools down, quenching the burn.

OMEGA implosion performance can be assessed by inferring the Lawson parameter from experimental observables and then extrapolating it to larger target sizes and greater laser energies[98]. To compare the present performance of direct drive with indirect drive, we consider recent cryogenic implosions that achieved the highest compression so far[27] and extrapolate their performance to the laser energy of 1.9 MJ used on the NIF. The pressure is inferred[15] from the neutron yield Y_N using the simple relation $Y_N \sim P^2(\langle\sigma v\rangle/T^2)V_{hs}\tau$, where V_{hs} is the hotspot volume, $\langle\sigma v\rangle$ is the fusion reactivity, and τ is the fusion burn duration. For instance, OMEGA shot 77068 (ref. 27, 28) achieved a pressure of about 56($\pm$7) Gbar at a temperature of 3.6 keV, with a total neutron yield of 5.2×10^{13}. The time history of the neutron production[99] shows that the burst of fusion reactions occurs over a time interval of about 68($\pm$10) ps. The burn duration is a good measure of the energy confinement time and, for this shot, the Lawson parameter is $P\tau \approx 3.8$ atm s. Because the pressure is mostly a function of the implosion velocity and the shell adiabat[6], implosions carried out on larger laser facilities with the same velocity and adiabat but larger target size would achieve the same pressure as on OMEGA. However, larger targets confine the pressure over longer times because of their greater target mass, and therefore the inertial confinement time is proportional to the target size.

Hydrodynamic scaling[98] is used to extrapolate the performance of OMEGA targets to larger energies. Hydrodynamic equivalent targets exhibit the same implosion velocity and adiabat. To keep the same velocity, the mass and volume are set proportional to the laser energy E_L, thereby leading to the target size (radius and thickness) scaling as $E_L^{1/3}$. Hydro-equivalent targets exhibit the same hydrodynamic stability properties by keeping the linear growth factors of the instabilities approximately equal across all target sizes[98]. It follows that the burn duration or confinement time τ scales proportionally to $E_L^{1/3}$. A 26-kJ OMEGA implosion scaled up to 1.9 MJ of laser energy would increase its confinement time by about 4.2$\times$ (ref. 28) and the Lawson parameter of shot 77068 scaled to 1.9 MJ is about $P\tau \simeq 16$ atm s. The central temperature inside the hotspot of ICF implosions depends weakly on target size. A small improvement in the temperature is predicted at larger sizes because of improved volume-to-surface ratio. According to ref. 6, the temperature scales as $E_L^{0.07}$, leading to a temperature improvement at 1.9 MJ of about 1.35$\times$, giving an extrapolated temperature for OMEGA shot 77068 of about 4.9 keV. The blue region in Fig. 2 shows the Lawson parameter and ion temperature of recent OMEGA cryogenic implosions extrapolated to 1.9 MJ. The expected level of alpha heating at 1.9 MJ of laser energy for direct drive is similar to present indirect-drive results with a fusion yield amplification from alpha heating of about 2$\times$ (ref. 28).

The yield amplification from alpha heating is a measure of the overall performance with respect to progress towards achieving burning-plasma conditions. Comparable values of the yield amplification for both direct and indirect drive indicate that both approaches have reached similar levels of performance, with a Lawson parameter slightly higher for indirect drive. It is important to emphasize that the alpha heating results for direct drive rely on extrapolations from OMEGA based solely on the hydrodynamic scaling. The extrapolation does not account for the changes in the growth of laser–plasma instabilities occurring at different scales. It also does not account for the differences in the seeds of the hydrodynamic instabilities and/or the low-mode asymmetries. Laser–plasma instabilities are expected to worsen at larger scales, because the threshold for parametric instabilities, such as the two-plasmon-decay instability (TPD)[25,100], is inversely proportional to the scale length of the coronal plasma[101]. In direct drive, hydrodynamic instabilities are mostly seeded by the DT ice roughness on the inner shell surface and by the laser-intensity speckles imprinting nonuniformities on the shell outer surface[23]. Although the relative magnitude of the ice roughness with respect to the target size is expected to improve at larger scales, the level of laser imprinting[23] is strongly dependent on the effectiveness of the adopted laser-smoothing technique[102,103]. Laser-smoothing techniques such as smoothing by spectral dispersion (SSD)[102] and induced spatial incoherence (ISI)[103] use broadband light to produce time-dependent phase-front variations through the laser beam. Effectively, as a result of laser smoothing, the laser-intensity nonuniformities fluctuate in time, and the speckle structure becomes smoothed when averaged over several coherence times. For instance, the laser smoothing on OMEGA, using two-dimensional SSD with a 1 THz bandwidth[104], is far superior to the present laser smoothing on the NIF, which uses one-dimensional SSD with a bandwidth of only 90 GHz. Implementation of multifrequency modulators on the NIF has been proposed as a simple modification to improve the laser-smoothing rates at lower total bandwidth[105]. Another assumption made in the extrapolation is that the laser configuration be the same, thereby implying that OMEGA symmetric illumination is maintained at different scales. This would not be the case for the NIF laser in the existing polar configuration, which is optimized for indirect drive. Therefore the OMEGA-to-NIF extrapolation described above assumes that the NIF be reconfigured for symmetric illumination. If the hydrodynamic scaling is preserved at different laser energies, then direct-drive implosions are expected to achieve high fusion yields for comparable alpha-heating levels. This is caused by the larger fuel mass assembled in direct-drive implosions with respect to indirect drive. A simple extrapolation of the fusion yields for hydro-equivalent targets without accounting for α-particle energy deposition leads to the simple scaling $Y_N^{no\alpha} \sim E_L^{1.45}$ (refs 28,98), indicating that OMEGA shot 77068 extrapolated to 1.9 MJ and with a two-fold amplification from alpha heating would produce about 5×10^{16} neutrons and more than 100 kJ of fusion energy[28].

Despite the progress made in laser smoothing, target fabrication and overall implosion performance, the path to ignition for direct drive presents significant challenges. One of the main mechanisms of performance degradation is the reduction of laser-energy absorption caused by cross-beam energy transfer (CBET). In direct drive, CBET reduces the coupling of laser energy to the target[106,107]. Outgoing laser rays of refracted light can interact with incoming central normal rays of incident beams, extracting their energy, and decreasing the overall laser-energy absorption (Fig. 5). In OMEGA implosions, CBET is thought to be responsible for more than a $\sim$ 20% reduction in laser energy coupled to the target[107]. Recent estimates indicate that CBET mitigation is required for a viable path to direct-drive ignition[108]. Different approaches have been proposed for CBET mitigation in direct drive, including wavelength detuning

between crossing beams[107] and zooming of beams to reduce beam crossing during the main portion of the laser pulse[107,109]. Recent experiments on OMEGA have demonstrated that decreasing the laser spot size on target significantly improves the laser-energy coupling to the target, at the price of increased nonuniformities[27]. Another improvement in implosion performance can be achieved by reducing the level of laser nonuniformities on target. Recent experiments have demonstrated that high-Z dopant in the ablator[110] or a thin high-Z coating[111] on the ablator surface significantly mitigate laser imprinting without changing the shell adiabat.

Another mechanism of compression degradation that can severely limit the implosion performance at larger energy scales is the hot-electron preheating from the TPD instability[100,112,113]. Significant progress has been made in recent years with regard to the characterization of the TPD instability and hot-electron generation in OMEGA implosions[114–117], as well as in the predictive capability of the TPD evolution[118,119]. Although an understanding of the hot-electron transport in the coronal plasma and energy deposition in the fuel is not yet complete, there are strong indications that hot-electron preheating is only of marginal importance for cryogenic implosions with plastic ablators on OMEGA at intensities below 10^{15} W cm^{-2}. At in-flight adiabats of $\sim$4, the areal density measured in cryogenic OMEGA implosions is similar to the values predicted by one-dimensional simulations, indicating that hot-electron preheat does not cause significant performance degradation at such adiabats and laser intensities[27]. At NIF scales, the TPD instability is expected to be driven more strongly owing to the longer plasma scale length. However, preliminary experiments[91] on the NIF designed to measure hot-electron production at long scale length have not shown a significant increase in the hot-electron fraction ($f_{\rm hot}$ = energy in hot electrons/laser energy) with respect to OMEGA experiments. A promising approach in reducing hot-electron preheat at NIF scales is to use ablators with atomic number greater than plastic CH. It has been shown in simulations[120] and experiments[121,122] that glass (SiO_2) and Al ablators produce lower amounts of hot electrons than plastic. Ignition target designs using mid-Z ablators have been recently investigated[123]. However, ablators with large atomic numbers have low hydrodynamic efficiency, thereby reducing the conversion of laser energy to shell kinetic energy. Multi-layered targets have been designed[108] to ablate a mid-Z silicon plasma into the corona where the TPD is localized while keeping an efficient low-Z ablator (Be) on the shell outer surface. A focused collaborative effort between LLE, LLNL and NRL is at present underway to improve the performance of direct-drive implosions, with the goal of achieving higher pressures on OMEGA that scale to ignition at about 2 MJ of laser energy (hydro-equivalent ignition). The main goals of this effort are to reduce the on-target laser nonuniformities, to improve the target quality with respect to surface roughness and other sources of nonuniformities, to control hot-electron preheat and to mitigate the effects of cross-beam energy transfer (CBET). Although the path to ignition is still uncertain, recent results on CBET mitigation and moderately high compression (over 50 Gbar) are promising and encouraging.

Advanced ignition schemes

Like direct and indirect drive, alternative laser ICF schemes use implosions of similar DT-filled capsules. They are typically referred to as advanced ignition schemes because they make use of external means to increase the temperature of the DT fuel and trigger ignition. These can be energetic particle beams (fast ignition), spherically convergent shocks (shock ignition), or externally applied magnetic fields (magnetized ICF and magneto-inertial fusion, or MIF). Magnetized ICF refers to conventional laser ICF with targets embedded in a magnetic field. Magneto-inertial fusion refers to a more general fusion concept that involves compression and magnetization of targets. Most MIF concepts use an electromagnetic driver for the implosion, and are not discussed here. Among the many MIF concepts studied over several decades, the recently proposed magnetized liner inertial fusion (MagLIF) scheme uses lasers for the initial heating of the fuel, and an electromagnetic driver for the implosion. In this section, we briefly review the status of inertial fusion via fast ignition, shock ignition, magnetized ICF and MagLIF.

Fast ignition. In fast ignition (FI)[29] the target is compressed to high densities with a low implosion velocity and then ignited by a high-intensity pulse of electrons or ions. Fast ignition has two potential advantages over conventional hotspot ignition: higher gains and less stringent symmetry requirements. Because FI targets are ignited by a particle beam, the compressed core pressure can be significantly less than for conventional ICF. Therefore, FI targets use massive shells of DT fuel driven at low implosion velocities, thereby allowing for larger energy gains[124]. Furthermore, because ignition does not depend on the central hotspot properties, FI does not require uniform implosions.

The FI concept[29] followed from the emergence of ultrahigh-intensity, short-pulse lasers (Fig. 6). The target compression is attained with a conventional high-energy laser driver (in direct or indirect drive) whereas the ignition is initiated by a fast laser pulse (the so-called ignitor or heating pulse), which produces a high-energy electron or ion beam when interacting with the target. Ignition is triggered in the dense fuel by the intense localized heating from the collimated particle beam. An overview of the FI concept can be found in ref. 125, and a summary of recent results is provided in ref. 126.

A number of different schemes for coupling a high-energy, short-pulse laser to a compressed core have been proposed. The hole-boring scheme[29] uses two short-pulse laser beams, one having a few hundred picosecond duration to create a channel in the coronal plasma through which the high-intensity laser pulse would propagate and accelerate electrons to MeV energies. An alternative design uses a hollow Au cone inserted in the spherical shell (cone-in-shell targets[127] shown in Fig. 6). The shell is compressed by the high-energy laser at the tip of the cone, whereas the hollow cone enables the short-pulse-ignition laser to propagate inside the cone without having to interact with the coronal plasma. Fast electrons are produced at the cone tip, very close to the dense plasma. Fast-ignition schemes using energetic electrons are usually referred to as electron FI. A variant cone-in-shell concept uses a thin foil to generate a jet of protons with multi-MeV energies (proton FI[128]). The protons deliver their energy to the fuel and initiate the ignition process. In proton FI, the loss of efficiency in the conversion of hot electrons into energetic protons is balanced by the ability to focus the protons onto a small spot.

At present, cone-guided electron FI is the most developed, and its ignition requirements on core compression and fast-electron beam properties have been well known since the late 1990s[129]. Various experiments have been carried out at large and small laser facilities. The most recent integrated experiments combining both target implosion and fast-electron heating have been fielded on the FIREX laser facility at Osaka University Institute for Laser Engineering (ILE) and on the OMEGA facility at the University of Rochester Laboratory for Laser Energetics (LLE). Both facilities include a long-pulse implosion laser (Gekko XII at ILE and OMEGA at LLE) and a short-pulse petawatt laser (LFEX at ILE and OMEGA EP at LLE). Experiments on both facilities have used cone-in-shell targets with a deuterated-plastic (CD) shell and a gold cone (Fig. 6). The main objective of these experiments was to demonstrate that fast electrons from the petawatt pulse were reaching the imploded CD capsule and heating it, thereby enhancing the fusion yield from the DD reactions in the compressed core.

The results of the initial integrated experiments at ILE[127] were confirmed in 2010 on FIREX[32] with a slight increase in ion

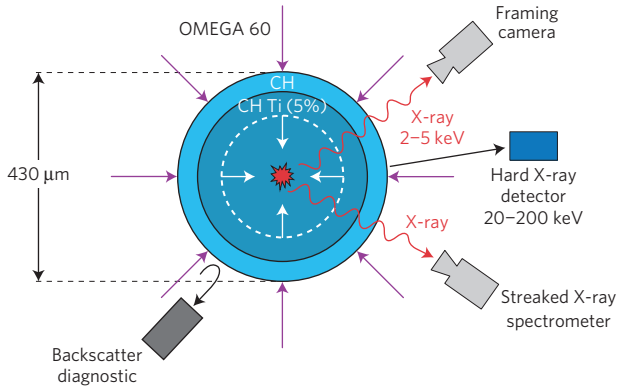

Figure 7 | OMEGA shock-ignition experiments. Experimental set-up for the spherical strong shock experiments on the OMEGA laser. A convergent shock launched by the 60 beams of OMEGA produces a flash of X-rays on convergence in the centre of a solid target. The shock-driving pressure is inferred from the timing of the X-ray flash. Figure reproduced from ref. 33, APS.

temperature and neutron yield. The 2010 experiments on FIREX used 500-μm-diameter, 7-μm-thick CD shells imploded by 2.5 kJ of 0.53-μm light from the Gekko XII laser. Two short-pulse (1.5 ps) 1.05-μm-wavelength beams delivered about 300 J on target, raising the neutron yield from 10^6 (without heating beams) to 3.5×10^7. The integrated FI experiments[31] on OMEGA used bigger targets, and greater compression and heating energies than the Osaka experiments. The targets were 870-μm-diameter, 40-μm-thick CD shells with an inserted gold cone. The shell compression was driven by 54 ultraviolet beams of OMEGA, delivering about 18 kJ on target, and it was first optimized in dedicated compression-only experiments[130]. The OMEGA EP 1.05-μm-wavelength short pulse, with an energy of about 1 kJ and a 10-ps duration, was focused with an average intensity $\sim 6 \times 10^{18}$ W cm^{-2} inside the cone. The highest neutron yield was about 1.8×10^7 (after subtraction of the $\sim 7 \times 10^6$ neutrons from the hot plasma ablated off the imploding shell), roughly four times larger than the neutron yield without heating beam[31].

The major challenges for FI are in controlling the energy and the divergence[131] of the fast electrons. Fast-electron energy and divergence are strongly affected by the tenuous plasma filling the cone before the arrival of the short pulse. The pre-plasma is formed by the interaction of a low-intensity long pre-pulse propagating ahead of the main high-intensity short pulse. The interaction of the short pulse with a large pre-plasma leads to the generation of electrons with energies of several MeV that are too energetic to efficiently couple their energy to the compressed core. Recent experiments on OMEGA use a visualization technique of fast-electron spatial energy deposition[132]. The new platform combines narrow bandwidth X-ray imaging and K-α spectroscopy measurements with a Cu-doped shell attached to a gold cone. These experiments[132] showed that the fast-electron production is distributed over the pre-plasma, with a large (~100 μm) stand-off distance between the critical density and the solid density cone tip, rather than localized at the cone tip. K-α imaging of the compressed cone-in-shell target showed that the hot-electron source exhibits a large divergence, with most electrons directed towards the cone sidewalls rather than in the forward direction. An optimized design with a larger cone tip of 40 μm (instead of 10 μm), an empty shell, and a high-contrast laser pulse was predicted to reduce the effects of the pre-plasma by moving the short-pulse interaction region closer to the cone tip, and by forming a higher-density core (due to the delayed cone tip breakout time with the empty shell). Experiments[132] with this improved target design and contrast ratio showed an increase in K-α yield by up to 4× and the energy coupling to the core was estimated at ~5–7%, the best coupling efficiency in OMEGA integrated experiments with 1 kJ of short-pulse energy.

Externally applied[133] or self-generated-resistive[134] magnetic fields can be used to improve the collimation of the fast electrons in fast-ignition targets. For a modest value of the fast-electron source stand-off distance of about ~ 70 μm from the compressed core, recent hybrid particle-in-cell (PIC) simulations[133] indicate that fast-electron energies greater than 1 MJ are not enough to ignite the dense fuel when the electron beam is highly divergent. Those simulations use an electron source with a divergence of about 52° (in the average velocity-space angle) obtained from pure three-dimensional PIC simulations. A magnetic field of 50 MG through the fast-electron source region[133] would greatly reduce the ignition energy to the same level of a collimated electron beam with only 10° divergence. Owing to the strong dependence of the ignition energy on the fast-electron divergence[135], significant improvements to the electron collimation are a necessary requirement for making progress in fast-ignition research.

Shock ignition. Like FI, shock ignition (SI) separates the compression of the thermonuclear fuel from the ignition trigger. The ignition process is initiated by a spherically convergent strong shock (the ignitor shock) launched at the end of the compression pulse. This late shock collides with the return shock driven by the rising pressure inside the central hotspot, thereby producing an ultrastrong gigabar shock that enhances the hotspot pressure and triggers the ignition process[30]. Without using the two-shock collision, ignition via direct heating by a spherical shock[136] would require driving pressures that cannot be achieved with existing laser technology. Shock ignition targets are thick shells imploded at relatively low implosion velocities (~200–300 km s^{-1}) and low intensities (mid-10^{14} W cm^{-2}) on a low adiabat to achieve high areal densities. The ignitor shock is launched by a spike in laser power at the end of the assembly pulse. The ignitor-shock-launching pressure needs to exceed 300 Mbar to provide a robust compression of the hot spot. For this reason, the laser intensity in the late power spike needs to be in the range 5×10^{15}–10^{16} W cm^{-2}. Two recent reviews of shock ignition describe SI implosion physics principles[137] and laser–plasma interaction physics[138]. Detailed SI target design studies have been carried out for the NIF[139], KrF lasers[140] and for the HiPER project[141]. Gain curves[142,143] and robustness studies[144] for SI point to the possibility of achieving high gains with relatively low laser energies.

The first implosion experiments using plastic CH shells filled with DT gas imploded by a ~19 kJ shaped pulse on the OMEGA laser showed that SI pulse shapes with a late power spike performed better than conventional pulse shapes with equal energy, leading to a ~4× increase in the fusion yield[145]. In these experiments, because of the power limitations of OMEGA, the late shock strength was well below the SI requirements for ignition, owing to a low spike intensity of about $8–9 \times 10^{14}$ W cm^{-2}. Because a critical issue for SI is the capability of launching shocks at pressures above 300 Mbar, multiple experiments were carried out at high intensities $\leq 10^{16}$ W cm^{-2} to demonstrate the generation of strong shocks. A first set of experiments at the LULI laser on planar targets measured shock-launching pressures of up to ~40 Mbar (ref. 146). Subsequently, planar experiments on OMEGA EP[147] and PALS[148] demonstrated launching of up to ~75 and ~90 Mbar shocks, respectively. Only recently, spherical strong shock (SSS) experiments[33,149] in solid plastic spheres on OMEGA at laser intensities up to 6×10^{15} W cm^{-2} and laser energies up to 27 kJ (Fig. 7) succeeded in launching shocks at pressures exceeding 300 Mbar. By eliminating the lateral heat losses occurring in the coronal plasma of planar targets, the spherical experiments were able to produce ablation pressures up to 400 Mbar. In these experiments, the shock pressures were not directly measured, but inferred from the X-ray flash time. The latter is the time of shock

convergence when a flash of X-rays is produced from a small ∼20-μm central region and measured with an X-ray framing camera. The earlier the X-ray flash occurs, the stronger the shock. A large signal in the hard X-ray detector (HXRD) from hot electrons slowing down in the target was observed. The hot-electron temperature and energy were inferred from the HXRD signal, leading to $T_{hot} \sim 50$–80 keV and E_{hot} over ∼2 kJ in plastic targets. Hot-electron generation was correlated with the measured backscattered light from stimulated Raman scattering (SRS)[149], and was higher when the SSD laser smoothing was turned off. Radiation hydrodynamic simulations including the inferred hot-electron population and slowing down (to reproduce the HXR signal) indicate that the hot-electron energy deposited onto the target significantly enhances the shock strength. This was confirmed by the earlier X-ray flash time from the shock convergence to the target centre that was observed when SSD was turned off. Adding the pressure enhancement from the hot-electron deposition to the ablation pressure led to estimating an equivalent shock-launching pressure up to 500 Mbar in these experiments[33]. In the presence of hot electrons, the equivalent shock-launching pressure is defined as the laser-induced ablation pressure required to drive the same shock, but without the pressure enhancement from the hot electrons. This equivalent pressure is found by repeating the simulation without including hot electrons, but artificially enhancing the laser ablation pressure by increasing the flux limiter (that is, increasing the heat flux from the laser deposition region to the ablation front). The measured hot-electron temperature in the SSS experiments was higher than in previous experiments at similar intensities where 20 beams of OMEGA were focused at high intensities onto a spherical shell imploded at low laser intensity by the remaining 40 beams[150]. In these 20 + 40 beam experiments, the high-intensity beams had a tight focal spot that minimized the beam overlap (single-beam interaction). For single-beam interaction experiments, the hot-electron energy was measured to be in the 30–40 keV range. The idea of using hot electrons to augment the shock pressure was advanced early in the development of shock ignition[30,151]. More recently, detailed calculations of the electron energy deposition in the target were used to relate the ablation pressure to the hot-electron flux incident on the target surface[152,153].

Understanding the laser–plasma interactions at intensities in the 5×10^{15}–10^{16} W cm^{-2} range is crucial for assessing the viability of the shock ignition scheme. Large PIC simulations[154,155] have been carried out to study laser–plasma instabilities in shock ignition, and the simulation results are in general agreement with the experimental observations of a dominant SRS over TPD and moderate hot-electron temperatures. At SI-relevant intensity, a transition from collisional to collisionless absorption maintains high laser-energy-absorption fractions[156] and the TPD is predicted to exhibit an early saturation as a result of plasma cavitation[157]. Although hot electrons are beneficial to SI when the target areal density is high enough to slow them down near the outer surface, concerns remain that a uniform preheat of the fuel can occur[158] and degrade the implosion performance. A significant effort is at present underway at the University of Bordeaux to develop a comprehensive radiation hydrodynamic code that includes a self-consistent source of hot electrons from the laser–plasma instability processes relevant to shock ignition[159].

Magneto-inertial fusion. Magneto-inertial fusion relies on the reduction of electron thermal conductivity and α-particle range perpendicular to a magnetic field, caused by gyration of charged particles around field lines, to relax the compression requirements for ICF. The magnetic fields required are far higher than what can be generated by conventional means ($>kT$ or 10 MG), so are attained by compressing a moderate external magnetic field (10–30 T or 0.1–0.3 MG) with the fuel. The requirement for efficient compression means that the magnetic pressure must remain much lower than the fuel pressure; a constraint which means that the ion thermal conductivity can be significantly suppressed only at temperatures close to the ignition conditions. At present, there are two distinct approaches to the use of magnetic field in ICF. The first is by improving the performance of conventional ICF implosions (magnetized ICF) and the second is by using low-implosion-velocity, low-convergence-ratio, cylindrical implosions that could only reach ignition with magnetization. The first approach has been demonstrated on the OMEGA laser using a single MIFEDS (magneto-inertial fusion electrical discharge system[160]) to provide magnetic fields from 6 to 14 T in deuterium-gas-filled, plastic spheres. Initial[161,162] and subsequent experiments showed a 15% increase in neutron-averaged ion temperature and a 30% increase in neutron yield due to the magnetic field. A straight magnetic field in a spherical target can reduce heat loss from the fuel over only half of its surface area, as thermal conductivity parallel to the field is unaffected. To correctly account for the reduction in thermal losses due to the magnetic field, two-dimensional simulations with anisotropic thermal conduction are required. A simplistic one-dimensional model describing the magnetic thermal insulation is to assume a uniform effective reduction by 2× in electron thermal conductivity instead of the reduction by half in the area of heat conduction. This leads to a roughly 20% increase in temperature[163] and an approximately 40% increase in fusion yield. In practice, the magnetic field causes a loss of spherical symmetry that degrades the implosion[163] beyond the one-dimensional predictions, unless the implosion already suffers from more severe symmetry issues. The increase in temperature means that the final pressure is reached at lower densities with slightly reduced convergence ratios, thereby reducing asymmetries and instability growth. Two-dimensional, magnetohydrodynamic (MHD) modelling of the NIC target with the addition of axial magnetic fields of 20–100 T has shown that the inner surface roughness required to prevent ignition is increased by the magnetic field as a result of the lower convergence required[164]. The resulting reduction in ρR is more than compensated by the reduction in α-particle range by the magnetic field. These results indicate that magnetic field could be used to restore the gain of a conventional ICF implosion that has become marginal owing to hydro instabilities, which may be the case for the NIC targets. The addition of an axial magnetic field to indirect-drive laser-fusion targets could also reduce the effect of laser–plasma instabilities in the gas fill of the hohlraum, in particular stimulated Raman scattering (SRS)[25]. The reduction of electron thermal conductivity in the gas will increase its temperature, which increases the threshold laser intensity for SRS and means that a lower gas density could be used to hold back the wall, which would further increase the SRS threshold. Preliminary magnetized hohlraum experiments on OMEGA showed suppression of SRS by magnetic field, and subsequent experiments measured an increase in gas temperature due to magnetic field[165]. The addition of magnetic-field generation capabilities to the NIF is at present under study as a means to achieve ignition.

The second approach was considered in simplified theoretical models around 20 years ago[166], and it was established that a magnetized, cylindrical DT plasma can self-heat at arbitrarily low values of ρR if the Larmor radius of the α-particles is slightly less than the fuel radius, corresponding to a field-radius product BR > 0.6 T m, although in moving to low ρR the temperature required increases from 4.5 keV to 7 keV. The first, detailed, practicable scheme involving lasers was proposed in 2010 by Slutz *et al.*[35] (Fig. 8a) from Sandia National Laboratories (SNL), who named it MagLIF (magnetized liner inertial fusion). In their proposal, a 30-T axial magnetic field is applied to a 7-mm-outer-diameter, 5-mm-long beryllium liner filled with 3 mg cm^{-3} of DT that is compressed by driving 27 MA of current through it in 100 ns, with the DT being preheated to 250 eV by a laser as it starts to compress (Fig. 8a). In one-dimensional MHD calculations,

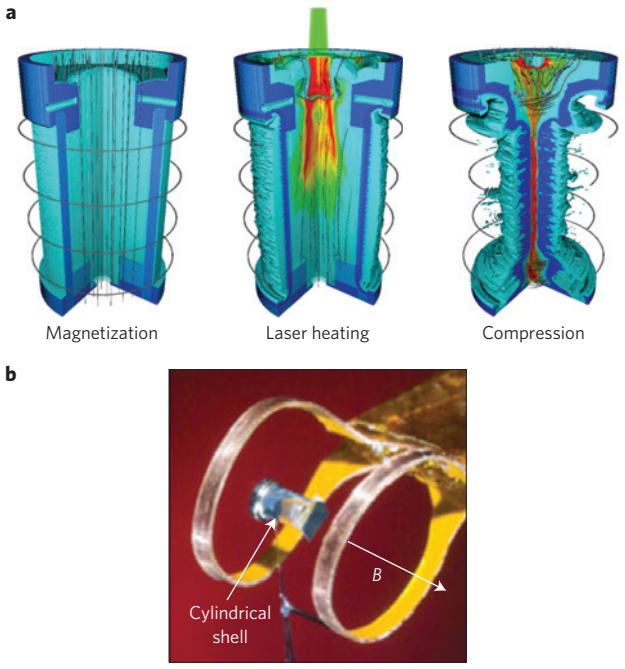

Figure 8 | Magnetic fields used in imploding targets. a, The three stages of a MagLIF implosion. **b**, A cylindrical target with Helmholtz coils for magnetic-field compression experiments on OMEGA. Panel **a** reproduced from ref. 36, APS.

this design gave 0.25 MJ of fusion yield, equal to half the kinetic energy coupled to the liner. The key innovation of MagLIF is preheating, which allows final temperatures greater than 7 keV to be achieved by a near-adiabatic, cylindrical compression at a convergence ratio less than 30. Suppression of electron heat flow by the axial magnetic field, which can be practically complete in a long enough cylinder, allows a near-adiabatic compression at implosion velocities as low as 70 km s^{-1}, limited by ion heat flow. Initial MagLIF experiments on the Z-machine at SNL, using a 10 T axial magnetic field, 19 MA drive and 2 kJ from the Z-beamlet laser, demonstrated fusion product confinement by the compressed magnetic field (tritium from deuterium–deuterium fusion in this case) and reached just less than half the temperature required for ignition[36], which is a major milestone for magneto-inertial fusion. However, neutron yields were 20 times lower than predicted by two-dimensional MHD calculations[167]. A possible explanation for the discrepancy between measured and predicted neutron yield is that the amount of laser energy coupled to the fuel during the preheating phase is significantly less than calculated using standard laser-energy deposition via collisional absorption. Laser–plasma instabilities in the unsmoothed beam of the Z-beamlet laser can greatly reduce the transmission of the laser beam through the entrance hole into the target. It is believed that laser preheating was significantly overestimated, and experiments studying just laser preheating confirm low energy coupling to the gas with the Z-beamlet laser. One-dimensional MHD calculations for MagLIF[168] indicate that DT fusion yields 100 times greater than the energy coupled to the target could be achieved for a 60 MA driver, which is a conceivable size for a successor to the Z-machine. For a pulsed-power driver, the energy coupled to the targets can be about 20% of the stored energy in the driver. Performance on Z experiments much closer to one-dimensional predictions will be required to justify this conclusion based on scaling Z implosion results to a 60 MA driver.

Magnetized cylindrical compression experiments (Fig. 8b) have been carried out on the OMEGA laser using MIFEDS since 2008[34], and demonstrated record magnetic-field compressions of just over 500 times. The only element of MagLIF that was missing was preheating, which could easily be provided by a single OMEGA beam. The drive energy available on OMEGA is 1,000 times lower than that available on Z, so the linear dimensions of an OMEGA laser-driven MagLIF target would have to be 10 times smaller than Z targets, so it could not achieve a field-radius product (BR) sufficient for confinement of fusion products. However, such an experiment would provide the first experimental data on MagLIF scaling, and yield more shots with better diagnostic access than on Z, which would greatly contribute to the basic physics understanding of MagLIF. In particular, the compressed axial magnetic field can be measured on OMEGA using proton probing[34], which is not possible on Z owing to the much larger azimuthal magnetic field used for the compression. For these reasons, a laser-driven MagLIF programme is at present underway on OMEGA, in collaboration with SNL. A series of experiments on OMEGA and OMEGA EP have shown that adequate preheating can be provided, considerably better than on the Z-beamlet laser because the OMEGA laser system uses 3ω rather than 2ω light (ω is the fundamental frequency) and has much smoother beams. Compression experiments on OMEGA without preheating and magnetic field have shown that a uniform, stable cylindrical compression can be achieved. The first full, laser-driven MagLIF experiments should be carried out on OMEGA towards the end of 2016. The NIF could also carry out laser-driven MagLIF experiments, if a magnetic-field capability is added, but such experiments would still be at ten times lower energy than the Z experiments, so would represent another step in understanding MagLIF scaling and the capability of laser-driven MagLIF, but could not reach ignition.

Conclusions

Although the path to thermonuclear ignition and energy gains with laser ICF is still uncertain, the demonstration of significant α-particle heating on the NIF indicates that, because of the threshold nature of ignition, moderate improvements in the implosion hydrodynamics could result in large increases in fusion yields. There are several important observations that can be made based on the results achieved thus far. The indirect-drive approach has demonstrated that it is possible to assemble thermonuclear fuel with a pressure of about 150–200 Gbar and temperature of about 5 keV using an imploding shell with only ∼15 kJ of kinetic energy and 170–180 μg of fuel mass. Although such pressures and temperatures are not sufficient to trigger ignition for such a small fuel mass, ignition at 150–200 Gbar and 5 keV should be possible if more mass is assembled, thereby increasing the inertial confinement time. One can use intensive quantities such as pressure and temperature to describe the 'quality' of an implosion, with fuel mass and core volume defining the 'size'. Ignition can be achieved by improving the quality of the implosion and/or by increasing its size. Increasing the size requires augmenting the kinetic energy of the imploding shell proportionally to its mass. Because up to 2 MJ of laser light is available at present on the NIF, of which only ∼15 kJ of kinetic energy is coupled to the fuel, it is clear that significant progress towards ignition can be made by improving the conversion from laser to fuel kinetic energy, which is now less than 1%. A significant effort is underway at present to explore strategies for improved energy coupling in indirect drive through more efficient hohlraums and ablator materials. Direct drive offers a straightforward path to improved energy coupling. It is expected that the core conditions of 150–200 Gbar and 5 keV demonstrated with indirect drive would be sufficient for ignition of the NIF-size directly driven targets with about 80–100 kJ of kinetic energy. However, direct-drive experiments on OMEGA have not yet achieved the same core pressures as indirect-drive experiments on NIF, indicating that, although direct drive has a size advantage, its implosion quality is below the level of indirect drive. A focused effort has begun to improve the implosion quality in direct drive, with a goal of demonstrating a core pressure in excess of 100 Gbar

at a temperature of 3.5–4 keV on the OMEGA laser. Such core conditions would scale favourably to achieving ignition at NIF laser energies, assuming that similar hydrodynamic properties can be attained on the NIF. In both direct and indirect drive, particular emphasis is devoted to improving the implosion quality by reducing the low-mode asymmetries that are thought to be an important factor in limiting the core pressure. An important question that future strategies in direct- and indirect-drive ICF should address, is whether or not we have enough control over the spatial–temporal deposition of laser energy and over the engineering quality of the targets to achieve ignition with the present levels of available energy that facilities can provide.

Although the conventional ICF approaches continue making progress towards improved implosion performance, alternative paths to ignition are being explored using an external trigger for ignition (particle beams or convergent shock waves) as well as externally applied magnetic fields. Significant progress has been made in recent years in all these approaches: fast ignition, shock ignition and magneto-inertial fusion. In terms of integrated performance, measured through fusion yields and ion temperature, alternative schemes lag behind conventional ICF. This is mostly due to the lack of suitable facilities, very limited shot-time allocations on existing facilities, and the reduced size of the effort devoted to alternative concepts. In the case of MagLIF, the initial results are promising, but too recent for a complete evaluation. For shock ignition, the results from the recent strong shock experiments (well above 300 Mbar) are encouraging, but uncertainties persist with respect to the understanding of laser–plasma interactions at shock-ignition-relevant laser intensities. For fast ignition, the issue of fast-electron collimation remains a major challenge to the viability of that scheme.

Received 22 December 2015; accepted 16 March 2016; published online 3 May 2016; corrected after print 1 June 2016

References

1. Nuckolls, J. *et al*. Laser compression of matter to super-high densities: thermonuclear (CTR) applications. *Nature* **239,** 139–142 (1972).
2. Atzeni, S. & Meyer-ter-vehn, J. *The Physics of Inertial Fusion* (Clarendon, 2004).
3. Lindl, J. D. *Inertial Confinement Fusion* (Springer, 1998).
4. Lawson, J. D. Some criteria for a power producing thermonuclear reactor. *Proc. Phys. Soc. Lond. B* **70,** 6–10 (1957).
5. Betti, R. *et al*. Thermonuclear ignition in inertial confinement fusion and comparison with magnetic confinement. *Phys. Plasmas* **17,** 058102 (2010).
6. Zhou, C. D. & Betti, R. Hydrodynamic relations for direct-drive fast-ignition and conventional inertial confinement fusion implosions. *Phys. Plasmas* **14,** 072703 (2008).
7. Glebov, V. Y. *et al*. Development of nuclear diagnostics for the National Ignition Facility. *Rev. Sci. Instrum.* **77,** 10E715 (2006).
8. Frenje, J. A. *et al*. Probing high areal-density cryogenic deuterium–tritium implosions using downscattered neutron spectra measured by the magnetic recoil spectrometer. *Phys. Plasmas* **17,** 056311 (2010).
9. Casey, D. T. *et al*. The magnetic recoil spectrometer for measurements of the absolute neutron spectrum at OMEGA and the NIF. *Rev. Sci. Instrum.* **84,** 043506 (2013).
10. Kishony, R. & Shvarts, D. Ignition condition and gain prediction for perturbed inertial confinement fusion targets. *Phys. Plasmas* **8,** 4925–4936 (2001).
11. Campbell, E. M. & Hogan, W. J. The National Ignition Facility—applications for inertial fusion energy and high-energy-density science. *Plasma Phys. Control. Fusion* **41,** B39 (1999).
12. Moses, E. I. Ignition on the National Ignition Facility. *J. Phys. Conf. Ser.* **112,** 012003 (2008).
13. Hurricane, O. A. *et al*. Fuel gain exceeding unity in an inertially confined fusion implosion. *Nature* **506,** 343–348 (2014).
14. Patel, P. *et al*. Performance of DT layered implosions on the NIF. in *55th Ann. Meet. APS Div. Plasma Phys.* NO4.00001 (American Physical Society, 2013); http://meetings.aps.org/link/BAPS.2013.DPP.NO4.1
15. Cerjan, C., Springer, P. T. & Sepke, S. M. Integrated diagnostic analysis of inertial confinement fusion capsule performance. *Phys. Plasmas* **20,** 056319 (2013).
16. Doeppner, T. *et al*. Demonstration of high performance in layered deuterium–tritium capsule implosions in uranium hohlraums at the National Ignition Facility. *Phys. Rev. Lett.* **115,** 055001 (2015).
17. Betti, R. *et al*. Alpha heating and burning plasmas in inertial confinement fusion. *Phys. Rev. Lett.* **114,** 255003 (2015).
18. Hurricane, O. A. *et al*. Inertially confined fusion plasmas dominated by alpha-particle self-heating. *Nature Phys.* http://dx.doi.org/10.1038/nphys3720 (2016).
19. Neiuport, J. *et al*. Design, optical characterization, and operation of large transmission gratings for the laser integration line and laser megajoule facilities. *Appl. Opt.* **44,** 3143–3152 (2005).
20. Boehly, T. R. *et al*. Initial performance results of the OMEGA laser system. *Opt. Commun.* **133,** 495–506 (1997).
21. Obenschain, S. P. *et al*. The Nike KrF laser facility: Performance and initial target experiments. *Phys. Plasmas* **3,** 2098–2107 (1996).
22. Gardner, J. H. & Bodner, S. E. Wavelength scaling for reactor-size laser-fusion targets. *Phys. Rev. Lett.* **47,** 1137–1140 (1981).
23. Bodner, E. S. *et al*. Direct-drive laser fusion: status and prospects. *Phys. Plasmas* **5,** 1901–1918 (1998).
24. Goncharov, V. N. *et al*. A model of laser imprinting. *Phys. Plasmas* **7,** 2062–2068 (2000).
25. Kruer, W. L. in *The Physics of Laser–Plasma Interactions, Frontiers in Physics* Vol. 73 (ed. Pines, D.) Ch. 6–8 (Addison-Wesley, 1988).
26. Kidder, R. E. Hot-electron preheat of laser-driven targets. *Nucl. Fusion* **21,** 145–151 (1981).
27. Regan, S. P. *et al*. Demonstration of 55 ± 7-Gbar hot-spot pressure in direct-drive layered DT cryogenic implosions on OMEGA. in *57th Ann. Meet. Div. Plasma Phys.* CI3.00005 (American Physical Society, 2015).
28. Bose, A. *et al*. Effects of long- and intermediate-wavelength nonuniformities on hot-spot energetics of hydrodynamic equivalent targets. in *57th Ann. Meet. Div. Plasma Phys.* GO5.00004 (American Physical Society, 2015).
29. Tabak, M. *et al*. Ignition and high gain with ultrapowerful lasers. *Phys. Plasmas* **1,** 1626–1634 (1994).
30. Betti, R. *et al*. Shock ignition of thermonuclear fuel with high areal density. *Phys. Rev. Lett.* **98,** 155001 (2007).
31. Theobald, W. *et al*. Initial cone-in-shell fast-ignition experiments on OMEGA. *Phys. Plasmas* **18,** 056305 (2011).
32. Azechi, H. *et al*. Present status of fast ignition realization experiment and inertial fusion energy development. *Nucl. Fusion* **53,** 104021 (2013).
33. Nora, R. *et al*. Gigabar spherical shock generation on the OMEGA laser. *Phys. Rev. Lett.* **114,** 045001 (2015).
34. Gotchev, O. V. *et al*. Laser-driven magnetic-flux compression in high-energy-density plasmas. *Phys. Rev. Lett.* **103,** 215004 (2009).
35. Slutz, S. A. *et al*. Pulsed-power-driven cylindrical liner implosions of laser preheated fuel magnetized with an axial field. *Phys. Plasmas* **17,** 56303 (2010).
36. Gomez, M. R. *et al*. Experimental demonstration of fusion-relevant conditions in magnetized liner inertial fusion. *Phys. Rev. Lett.* **113,** 155003 (2014).
37. Lindl, J. D. *et al*. The Physics basis for ignition using indirect-drive targets on the National Ignition Facility. *Phys. Plasmas* **11,** 339–491 (2004).
38. Haan, S. W. *et al*. Point design targets, specifications, and requirements for the 2010 ignition campaign on the National Ignition Facility. *Phys. Plasmas* **18,** 051001 (2011).
39. Lindl, J. *et al*. Review of the National Ignition Campaign 2009–2012. *Phys. Plasmas* **21,** 020501 (2014); erratum **21**, 129902 (2014).
40. Clark, D. S. *et al*. Radiation hydrodynamics modeling of the highest compression inertial confinement fusion ignition experiment from the National Ignition Campaign. *Phys. Plasmas* **22,** 022703 (2015).
41. Stadermann, M. *et al*. Improvements to Formvar tent fabrication using the meniscus coater. *Fusion Sci. Tech.* **59,** 58–62 (2011).
42. Haan, S. W. *et al*. Instability growth seeded by oxygen in CH shells on the National Ignition Facility. *Phys. Plasmas* **22,** 032708 (2015).
43. Regan, S. P. *et al*. Hot-spot mix in ignition-scale implosions on the NIF. *Phys. Plasmas* **19,** 056307 (2012).
44. Jones, O. S. *et al*. A high-resolution integrated model of the National Ignition Campaign cryogenic layered experiments. *Phys. Plasmas* **19,** 056315 (2012).
45. Edwards, M. J. *et al*. Progress towards ignition on the National Ignition Facility. *Phys. Plasmas* **20,** 070501 (2013).
46. Ma, T. *et al*. Onset of hydrodynamic mix in high-velocity, highly compressed inertial confinement fusion implosions. *Phys. Rev. Lett.* **111,** 085004 (2013).
47. Town, R. P. J. *et al*. Dynamic symmetry of indirectly driven inertial confinement fusion capsules on the National Ignition Facility. *Phys. Plasmas* **21,** 056313 (2014).
48. Moody, J. D. *et al*. Early time implosion symmetry from two-axis shock-timing measurements on indirect drive NIF experiments. *Phys. Plasmas* **21,** 092702 (2014).

49. Moody, J. D. *et al*. Progress in hohlraum physics for the National Ignition Facility. *Phys. Plasmas* **21,** 056317 (2014).
50. MacLaren, S. A. *et al*. Novel characterization of capsule X-ray drive at the National Ignition Facility. *Phys. Rev. Lett.* **112,** 105003 (2014).
51. Callahan, D. *et al*. Higher velocity, high-foot implosions on the National Ignition Facility laser. *Phys. Plasmas* **22,** 056314 (2015).
52. MacPhee, A. *et al*. Stabilization of high-compression indirect-drive inertial confinement fusion implosions using a 4-shock adiabat-shaped drive. *Phys. Plasmas* **22,** 080702 (2015).
53. Raman, K. S. *et al*. An in-flight radiography platform to measure hydrodynamic instability growth in inertial confinement fusion capsules at the National Ignition Facility. *Phys. Plasmas* **21,** 072710 (2014).
54. Peterson, J. L. *et al*. Validating hydrodynamic growth in National Ignition Facility implosions. *Phys. Plasmas* **22,** 056309 (2015).
55. Smalyuk, V. A. *et al*. Hydrodynamic instability growth of three-dimensional, "native-roughness" modulations in X-ray driven, spherical implosions at the National Ignition Facility. *Phys. Plasmas* **22,** 072704 (2015).
56. Casey, D. T. *et al*. Reduced instability growth with high-adiabat high-foot implosions at the National Ignition Facility. *Phys. Rev. E* **90,** 011102(R) (2014).
57. Dittrich, T. R. *et al*. Design of a high-foot/high-adiabat ICF capsule for the National Ignition Facility. *Phys. Rev. Lett.* **112,** 055002 (2014).
58. Peterson, J. L. *et al*. Differential ablator-fuel adiabat tuning in indirect-drive implosions. *Phys. Rev. E* **91,** 031101(R) (2015).
59. Park, H.-S. *et al*. High-adiabat, high-foot, inertial confinement fusion implosion experiments on the National Ignition Facility. *Phys. Rev. Lett.* **112,** 055001 (2014).
60. Hurricane, O. A. *et al*. The high-foot implosion campaign on the National Ignition Facility. *Phys. Plasmas* **21,** 056314 (2014).
61. Casey, D. *et al*. Improved performance of high areal density indirect drive implosions at the National Ignition Facility using a four-shock adiabat shaped drive. *Phys. Rev. Lett.* **115,** 105001 (2015).
62. Smalyuk, V. *et al*. First results of radiation-driven, layered deuterium–tritium implosions with a 3-shock adiabat-shaped drive at the National Ignition Facility. *Phys. Plasmas* **22,** 080703 (2015).
63. Mackinnon, A. J. *et al*. High-density carbon ablator experiments on the National Ignition Facility. *Phys. Plasmas* **21,** 056318 (2014).
64. Berzak Hopkins, L. F. *et al*. First high-convergence cryogenic implosion in a near-vacuum hohlraum. *Phys. Rev. Lett.* **114,** 175001 (2015).
65. Meezan, N. B. *et al*. Cryogenic tritium–hydrogen–deuterium and deuterium–tritium layer implosions with high density carbon ablators in near-vacuum hohlraums. *Phys. Plasmas* **22,** 062703 (2015).
66. Ross, J. S. *et al*. High-density carbon capsule experiments on the National Ignition Facility. *Phys. Rev. E* **91,** 021101(R) (2015).
67. Ma, T. *et al*. Thin-shell high-velocity ICF implosions on the National Ignition Facility. *Phys. Rev. Lett.* **114,** 145004 (2015).
68. Michel, P. *et al*. Tuning the implosion symmetry of ICF targets via controlled crossed-beam energy transfer. *Phys. Rev. Lett.* **102,** 025004 (2009).
69. Michel, P. *et al*. Symmetry tuning via controlled crossed-beam energy transfer on the National Ignition Facility. *Phys. Plasmas* **17,** 056305 (2010).
70. Moody, J. D. *et al*. Multistep redirection by cross-beam power transfer of ultrahigh-power lasers in a plasma. *Nature Phys.* **8,** 344–349 (2012).
71. Callahan, D. A. *et al*. The velocity campaign for ignition on NIF. *Phys. Plasmas* **19,** 056305 (2012).
72. Kritcher, A. *et al*. Integrated modeling of cryogenic layered high-foot experiments at the NIF. *Phys. Plasmas* (submitted, 2016).
73. Clark, D. S. *et al*. Three-dimensional simulations of low foot and high foot implosion experiments on the National Ignition Facility. *Phys. Plasmas* **23,** 056302 (2016).
74. Nagel, S. R. *et al*. Effect of the mounting membrane on shape in inertial confinement fusion implosions. *Phys. Plasmas* **22,** 022704 (2015).
75. Tommasini, R. *et al*. Tent-induced perturbations on areal density of implosions at the National Ignition Facility. *Phys. Plasmas* **22,** 056315 (2015).
76. Regan, S. P. *et al*. Suprathermal electrons generated by the two-plasmon-decay instability in gas-filled hohlraums. *Phys. Plasmas* **17,** 020703 (2010).
77. Kritcher, A. L. *et al*. Metrics for long wavelength asymmetries in inertial confinement fusion implosions on the National Ignition Facility. *Phys. Plasmas* **21,** 042708 (2014).
78. Spears, B. K. *et al*. Three-dimensional simulations of National Ignition Facility implosions: insight into experimental observables. *Phys. Plasmas* **22,** 056317 (2015).
79. Zylstra, A. B. *et al*. In-flight observations of low-mode ρR asymmetries in NIF implosions. *Phys. Plasmas* **22,** 056301 (2015).
80. Pak, A. *et al*. Laser absorbtion, power transfer, and radiation symmetry during the first shock of inertial confinement fusion gas-filled hohlraum experiments. *Phys. Plasmas* **22,** 122701 (2015).
81. Simakov, A. *et al*. Optimized beryllium target design for indirectly driven inertial confinement fusion experiments on the National Ignition Facility. *Phys. Plasmas* **21,** 022701 (2014).
82. Yi, S. A. *et al*. Hydrodynamic instabilities in beryllium targets for the National Ignition Facility. *Phys. Plasmas* **21,** 092701 (2014).
83. Clark, D. S. *et al*. A survey of pulse shape options for a revised plastic ablator ignition design. *Phys. Plasmas* **21,** 112705 (2014).
84. Baker, K. *et al*. Adiabat-shaping in indirect drive inertial confinement fusion. *Phys. Plasmas* **22,** 052702 (2015).
85. Milovich, J. *et al*. Design of indirectly driven, high-compression Inertial Confinement Fusion Implosions with improved hydrodynamic stability using a 4-shock adiabat-shaped drive. *Phys. Plasmas* **22,** 122702 (2015).
86. Robey, H. *et al*. Performance of indirectly driven capsule implosions on NIF using adiabat-shaping. *Phys. Plasmas* **23,** 056303 (2016).
87. Hinkel, D. E. *et al*. Improved hohlraums for high foot implosions. in *57th Ann. Meet. APS Div. Plasma Phys.* BO4.00004 (American Physical Society, 2015); http://meetings.aps.org/link/BAPS.2015.DPP.BO4.4
88. Leidinger, J.-P. *et al*. NIF Rugby High Foot Campaign from the design side. in *Proc. 9th Int. Conf. Inertial Fusion Sci. Appl. J. Phys. Conf. Ser.* Paper 174 (in the press).
89. Hohenberger, M. *et al*. Polar-direct-drive experiments on the National Ignition Facility. *Phys. Plasmas* **22,** 056308 (2015).
90. Radha, P. B. *et al*. Polar direct drive—simulations and results from OMEGA and the National Ignition Facility. in *57th Ann. Meet. Div. Plasma Phys.* CI3.00004 (American Physical Society, 2015).
91. Rosenberg, M. J. *et al*. Planar two-plasmon–decay experiments at polar-direct-drive ignition-relevant scale lengths at the National Ignition Facility. in *57th Ann. Meet. Div. Plasma Phys.* NO5.00006 (American Physical Society, 2015).
92. Stoeckl, C. *et al*. First results from cryogenic target implosions on OMEGA. *Phys. Plasmas* **9,** 2195–2201 (2002).
93. Sangster, T. C. *et al*. Improving cryogenic deuterium–tritium implosion performance on OMEGA. *Phys. Plasmas* **20,** 056317 (2013).
94. Goncharov, V. N. *et al*. Improved performance of direct-drive inertial confinement fusion target designs with adiabat shaping using an intensity picket. *Phys. Plasmas* **10,** 1906–1918 (2003).
95. Anderson, K. *et al*. Laser-induced adiabat shaping by relaxation in inertial fusion implosions. *Phys. Plasmas* **11,** 5–8 (2004).
96. Goncharov, V. N. *et al*. Demonstration of the highest deuterium–tritium areal density using multiple-picket cryogenic designs on omega. *Phys. Rev. Lett.* **104,** 165001 (2010).
97. Takabe, H. *et al*. Selfconsistent growth rate of the Rayleigh–Taylor instability in an ablatively accelerating plasma. *Phys. Fluids* **28,** 3676–3682 (1985).
98. Nora, R. *et al*. Theory of hydro-equivalent ignition for inertial fusion and its applications to OMEGA and the National Ignition Facility. *Phys. Plasmas* **21,** 056316 (2014).
99. Stoeckl, C. *et al*. Ten-inch manipulator-based neutron temporal diagnostic for cryogenic experiments on OMEGA. *Rev. Sci. Instrum.* **74,** 1713–1716 (2003).
100. Seka, W. *et al*. Two-plasmon-decay instability in direct-drive inertial confinement fusion experiments. *Phys. Plasmas* **16,** 052701 (2009).
101. Simon, A. *et al*. On the inhomogeneous two-plasmon instability. *Phys. Fluids* **26,** 3107–3118 (1983).
102. Skupsky, S. *et al*. Improved laser-beam uniformity using the angular dispersion of frequency-modulated light. *J. Appl. Phys.* **66,** 3456–3462 (1989).
103. Lehmberg, R. H. & Obenschain, S. P. Use of induced spatial incoherence for uniform illumination of laser fusion targets. *Opt. Commun.* **46,** 27–31 (1983).
104. Regan, S. P. *et al*. Performance of 1-THz-bandwidth, two-dimensional smoothing by spectral dispersion and polarization smoothing of high-power, solid-state laser beams. *J. Opt. Soc. Am. B* **22,** 998–1002 (2005).
105. Collins, T. J. B. *et al*. A polar-drive ignition design for the National Ignition Facility. *Phys. Plasmas* **19,** 056308 (2012).
106. Igumenshchev, I. V. *et al*. Crossed-beam energy transfer in implosion experiments on OMEGA. *Phys. Plasmas* **17,** 122708 (2010).
107. Igumenshchev, I. V. *et al*. Crossed-beam energy transfer in direct-drive implosions. *Phys. Plasmas* **19,** 056314 (2012).
108. Goncharov, V. *et al*. Improving the hot-spot pressure and demonstrating ignition hydrodynamic equivalence in cryogenic deuterium–tritium implosions on OMEGA. *Phys. Plasmas* **21,** 056315 (2014).
109. Froula, D. H. *et al*. Mitigation of cross-beam energy transfer: implication of two-state focal zooming on OMEGA. *Phys. Plasmas* **20,** 082704 (2013).
110. Hu, S. *et al*. Mitigating laser imprint in direct-drive inertial confinement fusion implosions with high-z dopants. *Phys. Rev. Lett.* **108,** 195003 (2012).
111. Karasik, M. *et al*. Suppression of laser nonuniformity imprinting using a thin high-z coating. *Phys. Rev. Lett.* **114,** 085001 (2015).
112. Smalyuk, V. A. *et al*. Role of hot-electron preheating in the compression of direct-drive imploding targets with cryogenic D2 ablators. *Phys. Rev. Lett.* **100,** 185005 (2008).

113. Sangster, T. C. *et al*. High-areal-density fuel assembly in direct-drive cryogenic implosions. *Phys. Rev. Lett.* **100,** 185006 (2008).
114. Seka, W. *et al*. Nonuniformly driven two-plasmon-decay instability in direct-drive implosions. *Phys. Rev. Lett.* **112,** 145001 (2014).
115. Follett, R. K. Direct observation of the two-plasmon-decay common plasma wave using ultraviolet Thomson scattering. *Phys. Rev. E* **91,** 031104(R) (2015).
116. Michel, D. T. *et al*. Experimental validation of the two-plasmon-decay common-wave process. *Phys. Rev. Lett.* **109,** 155007 (2012).
117. Froula, D. H. *et al*. Saturation of the two-plasmon decay instability in long-scale-length plasmas relevant to direct-drive inertial confinement fusion. *Phys. Rev. Lett.* **108,** 165003 (2012).
118. Yan, R. *et al*. Generating energetic electrons through staged acceleration in the two-plasmon-decay instability in inertial confinement fusion. *Phys. Rev. Lett.* **108,** 175002 (2012).
119. Zhang, J. *et al*. Multiple beam two-plasmon decay: linear threshold to nonlinear saturation in three dimensions. *Phys. Rev. Lett.* **113,** 105001 (2014).
120. Myatt, J. F. *et al*. Mitigation of two-plasmon decay in direct-drive inertial confinement fusion through the manipulation of ion-acoustic and Langmuir wave damping. *Phys. Plasmas* **20,** 052705 (2013).
121. Smalyuk, V. *et al*. Implosion experiments using glass ablators for direct-drive inertial confinement fusion. *Phys. Rev. Lett.* **104,** 165002 (2010).
122. Froula, D. H. *et al*. Laser–plasma interactions in direct-drive ignition plasmas. *Plasma Phys. Control. Fusion* **54,** 124016 (2012).
123. Lafon, M. *et al*. Direct-drive ignition designs with mid-Z ablators. *Phys. Plasmas* **22,** 032703 (2015).
124. Betti, R. & Zhou, C. D. High-density and high-ρR fuel assembly for fast-ignition inertial confinement fusion. *Phys. Plasmas* **12,** 110702 (2005).
125. Key, M. H. Status of and prospects for the fast ignition inertial fusion concept. *Phys. Plasmas* **14,** 055502 (2007).
126. Craxton, R. S. *et al*. Direct-drive inertial confinement fusion: a review. *Phys. Plasmas* **22,** 110501 (2015).
127. Kodama, R. *et al*. Nuclear fusion: fast heating scalable to laser fusion ignition. *Nature* **418,** 933–934 (2002).
128. Roth, M. *et al*. Fast ignition by intense laser-accelerated proton beams. *Phys. Rev. Lett.* **86,** 436–439 (2001).
129. Atzeni, S. Inertial fusion fast ignitor: igniting pulse parameter window vs the penetration depth of the heating particles and the density of the precompressed fuel. *Phys. Plasmas* **6,** 3316–3326 (1999).
130. Stoeckl, C. *et al*. Hydrodynamics studies of direct-drive cone-in-shell, fast-ignitor targets on OMEGA. *Phys. Plasmas* **14,** 112702 (2007).
131. Green, J. S. *et al*. Effect of laser intensity on fast-electron-beam divergence in solid-density plasmas. *Phys. Rev. Lett.* **100,** 015003 (2008).
132. Jarrott, L. C. *et al*. Visualizing fast electron energy transport into laser-compressed high-density fast-ignition targets. *Nature Phys.* http://dx.doi.org/10.1038/nphys3614 (2016).
133. Strozzi, D. *et al*. Fast-ignition transport studies: realistic electron source, integrated particle-in-cell and hydrodynamic modeling, imposed magnetic fields. *Phys. Plasmas* **19,** 072711 (2012).
134. Robinson, A. *et al*. Focusing of relativistic electrons in dense plasma using a resistivity-gradient-generated magnetic switchyard. *Phys. Rev. Lett.* **108,** 125004 (2012).
135. Bellei, C. *et al*. Fast ignition: dependence of the ignition energy on source and target parameters for particle-in-cell-modelled energy and angular distributions of the fast electrons. *Phys. Plasmas* **20,** 052704 (2013).
136. Shcherbakov, V. A. Ignition of a laser-fusion target by a focusing shock wave. *Sov. J. Plasma Phys.* **9,** 240–241 (1983).
137. Atzeni, S. *et al*. Shock ignition of thermonuclear fuel: principles and modelling. *Nucl. Fusion* **54,** 054008 (2014).
138. Batani, D. *et al*. Physics issues for shock ignition. *Nucl. Fusion* **54,** 054009 (2014).
139. Perkins, L. J. *et al*. Shock Ignition: a new approach to high gain inertial confinement fusion on the National Ignition Facility. *Phys. Rev. Lett.* **103,** 045004 (2009).
140. Schmitt, A. J. *et al*. Shock ignition target design for inertial fusion energy. *Phys. Plasmas* **17,** 042701 (2010).
141. Ribeyre, X. *et al*. Shock ignition: an alternative scheme for HiPER. *Plasma Phys. Control. Fusion* **51,** 015013 (2009).
142. Lafon, M. *et al*. Gain curves and hydrodynamic modeling for shock ignition. *Phys. Plasmas* **17,** 052704 (2010).
143. Atzeni, S. *et al*. Energy and wavelength scaling of shock-ignited inertial fusion targets. *New J. Phys.* **15,** 045004 (2013).
144. Ribeyre, X. *et al*. Shock ignition: modelling and target design robustness. *Plasma Phys. Control. Fusion* **51,** 124030 (2009).
145. Theobald, W. *et al*. Initial experiments on the shock-ignition inertial confinement fusion concept. *Phys. Plasmas* **15,** 056306 (2008).
146. Baton, S. D. *et al*. Experiment in planar geometry for shock ignition studies. *Phys. Rev. Lett.* **108,** 195002 (2012).
147. Hohenberger, M. *et al*. Shock-ignition relevant experiments with planar targets on OMEGA. *Phys. Plasmas* **21,** 022702 (2014).
148. Batani, D. *et al*. Generation of high pressure shocks relevant to the shock-ignition intensity regime. *Phys. Plasmas* **21,** 032710 (2014).
149. Theobald, W. *et al*. Spherical strong-shock generation for shock-ignition inertial fusion. *Phys. Plasmas* **22,** 056310 (2015).
150. Theobald, W. *et al*. Spherical shock-ignition experiments with the 40 + 20-beam configuration on OMEGA. *Phys. Plasmas* **19,** 102706 (2012).
151. Betti, R. *et al*. Shock ignition of thermonuclear fuel with high areal densities. *J. Phys. Conf. Ser.* **112,** 022024 (2008).
152. Piriz, A. R. *et al*. Ablation driven by hot electrons generated during the ignitor laser pulse in shock ignition. *Phys. Plasmas* **19,** 122705 (2012).
153. Gus'kov, S. *et al*. Ablation pressure driven by an energetic electron beam in a dense plasma. *Phys. Rev. Lett.* **109,** 255004 (2012).
154. Klimo, O., Weber, S., Tikhonchuk, V. T. & Limpouch, J. Particle-in-cell simulations of laser-plasma interaction for the shock ignition scenario. *Plasma Phys. Control. Fusion* **52,** 055013 (2010).
155. Yan, R. *et al*. Intermittent laser–plasma interactions and hot electron generation in shock ignition. *Phys. Plasmas* **21,** 062705 (2014).
156. Klimo, O. *et al*. Laser plasma interaction studies in the context of shock ignition—transition from collisional to collisionless absorption. *Phys. Plasmas* **18,** 082709 (2011).
157. Weber, S. *et al*. Fast saturation of the two-plasmon-decay instability for shock-ignition conditions. *Phys. Rev. E* **85,** 016403 (2012).
158. Nicolai, Ph. *et al*. Deleterious effects of nonthermal electrons in shock ignition concept. *Phys. Rev. E* **89,** 033107 (2014).
159. Tikhonchuck, V. *et al*. Multiscale models of laser–plasma interaction for the shock ignition scheme. in *9th Inertial Fusion Sic. Appl. Conf.* (2015).
160. Gotchev, O. V. *et al*. Seeding magnetic fields for laser-driven flux compression in high-energy-density plasmas. *Rev. Sci. Instrum.* **80,** 043504 (2009); Fiksel, G. *et al.* Note: experimental platform for magnetized high-energy-density plasma studies at the OMEGA laser facility. *Rev. Sci. Instrum.* **86** 016105 (2015).
161. Chang, P. Y. *et al*. Fusion yield enhancement in magnetized laser-driven implosions. *Phys. Rev. Lett.* **107,** 035006 (2011).
162. Hohenberger, M. *et al*. Inertial confinement fusion implosions with imposed magnetic field compression using the OMEGA laser. *Phys. Plasmas* **19,** 056306 (2012).
163. Davies, J. C., Betti, R., Chang, P. Y. & Fiksel, G. The importance of electrothermal terms in Ohm's law for magnetized spherical implosions. *Phys. Plasmas* **22,** 112703 (2015).
164. Perkins, L. J., Logan, B. G., Zimmerman, G. B. & Werner, C. J. Two-dimensional simulations of thermonuclear burn in ignition-scale inertial confinement fusion targets under compressed axial magnetic fields. *Phys. Plasmas* **20,** 072708 (2013).
165. Montgomery, D. S. *et al*. Use of external magnetic fields in hohlraum plasmas to improve laser-coupling. *Phys. Plasmas* **22,** 010703 (2015); erratum **22,** 079901 (2015).
166. Basko, M. M., Kemp, A. J. & Meyer-ter-Vehn, J. Ignition conditions for magnetized target fusion in cylindrical geometry. *Nucl. Fusion* **40,** 59–68 (2000).
167. Sefkow, A. B. *et al*. Design of magnetized liner inertial fusion experiments using the Z facility. *Phys. Plasmas* **21,** 072711 (2014).
168. Slutz, S. A. & Vesey, R. A. High-gain magnetized inertial fusion. *Phys. Rev. Lett.* **108,** 025003 (2012).

Acknowledgements

The authors would like to thank the US and the international ICF community for their continuing efforts to make inertial fusion in the laboratory a reality. Special thanks to J. R. Davies of LLE for his input on the Magneto-Inertial Fusion section of this manuscript. The authors are grateful to M. E. Campbell, S. P. Regan, T. C. Sangster and W. Theobald of LLE, F. Beg of UCSD, D. Sinar of SNL and to D. Clark, M. J. Edwards, L. F. Berzak-Hopkins, A. Kritcher and T. Ma of LLNL for reviewing this manuscript. This work was performed under the auspices of the US Department of Energy by Lawrence Livermore National Laboratory under Contract No. DE-AC52-07NA27344, by the University of Rochester Laboratory for Laser Energetics under Cooperative Agreements DE-NA0001944 (NNSA) and DE-FC02-04ER54789 (OFES), and with the support of the New York State Energy Research Development Authority.

Additional information

Reprints and permissions information is available online at www.nature.com/reprints. Correspondence should be addressed to R.B.

Competing financial interests

The authors declare no competing financial interests.

Corrigendum: Inertial-confinement fusion with lasers

R. Betti and O. A. Hurricane

Nature Physics **12,** 435–448 (2016); published online 3 May 2016; corrected after print 1 June 2016.

In the version of this Review Article originally published, the size of the gold hohlraum described in the section 'Laser indirect drive' was incorrect and it should have read '5.75 mm in diameter'. This has been corrected in the online versions after print 1 June 2016.